eLife

Reviewed Preprint
v1 • February 17, 2025
Not revised

Reviewed Preprint
v2 • June 25, 2026
Revised by authors

Parkinson's disease-associated *Pink1* loss disrupts ensheathing glia and causes dopaminergic neuron synapse loss

Lorenzo Ghezzi[1,2], Sabine Kuenen[1,2], Ulrike Pech[1,2], Nils Schoovaerts[1,2], Ayse Kilic[1,2], Suresh Poovathingal[1,2,3], Kristofer Davie[1,2], Jochen Lamote[1,3], Roman Praschberger[1,2,4] ✉, Patrik Verstreken[1,2] ✉

[1]VIB-KU Leuven Center for Neuroscience, Leuven, Belgium • [2]KU Leuven, Department of Neurosciences, Leuven Brain Institute, Leuven, Belgium • [3]VIB Flow Core Leuven, VIB Technologies, Leuven, Belgium • [4]Medical University of Innsbruck, Institute of Human Genetics, Innsbruck, Austria

✉ **For correspondence:**
roman.praschberger@i-med.ac.at
patrik.verstreken@kuleuven.be

Competing interests: P.V. is the scientific founder of Jay Therapeutics. All other authors declare no competing interests.

Funding: See page 26

Reviewing editor: Hugo J Bellen, Baylor College of Medicine, United States

eLife Assessment

This **valuable** study explores the role of Pink1 in regulating mitochondria-organelle contacts and glial function, advancing our understanding of the mechanisms underlying neurodegenerative diseases. The findings highlight key genes and cellular processes that are critical in maintaining neuronal health, with implications for glial biology and Parkinson's disease research. The methodology and data are **solid**. This work will be of significant interest to researchers in neuroscience, cell biology, and neurodegenerative diseases.

https://doi.org/10.7554/eLife.105386.2.sa3

Abstract

Parkinson's disease (PD) is commonly associated with the loss of dopaminergic neurons in the *substantia nigra*, but many other cell types are affected even before neuron loss occurs. Recent studies have linked oligodendrocytes to early stages of PD, though their precise role is still unclear. *PINK1* is mutated in familial PD, and through unbiased single-cell sequencing of the entire brain of *Drosophila Pink1* models, we observed significant gene deregulation in ensheathing glia (EG); cells that share functional similarities with oligodendrocytes. We found that the loss of *Pink1* leads to abnormalities in EG, similar to the reactive response of EG seen upon nerve injury. Using cell-type-specific transcriptomics, we identified deregulated genes in EG as potential functional modifiers. Specifically downregulating two trafficking factors in EG, *Vps35* and *Vps13*, also mutated in PD, was sufficient to rescue neuronal function and protect against dopaminergic synapse loss. Our findings demonstrate that *Pink1* loss in neurons triggers an injury-like response in EG, and that *Pink1* loss in EG in turn disrupts neuronal function. Vesicle trafficking components, which may regulate membrane interactions between organelles in EG, seem to play a role in maintaining neuronal health and ultimately preventing dopaminergic synapse loss. Our work highlights the essential role of glial support cells in the pathogenesis of PD and identifies vesicle trafficking within these cells in disease progression.

Introduction

Parkinson's disease (PD) is characterized by motor symptoms such as bradykinesia, rigidity and tremor that are caused by the progressive loss of dopaminergic neurons in the substantia nigra (Lang & Lozano, 1998). However, most of the patients report non-motor symptoms, such as constipation, hyposmia and sleep defects, even before the onset of motor symptoms (Munhoz et al., 2015). This suggests that PD is a progressive neurodegenerative disease that initiates many

years before the diagnosis and involves different neuronal systems, multiple anatomical areas and different cell types. While therapies symptomatically improve motor functioning temporarily by restoring dopaminergic tone, they do not effectively prevent neurodegeneration and disease progression. This highlights the necessity to identify cell-types and biological mechanisms that act at the earliest stages of disease.

With the advent of single-cell sequencing applied to PD and control brains in combination with evidence from genome-wide association studies (GWAS), it is now possible to identify which cells and mechanisms are at play in PD models that recapitulate early stages of PD (Kaempf et al., 2026; Pech et al., 2025). Among these, one study reported that genes related to GWAS loci are enriched for oligodendrocyte-specific gene expression (Bryois et al., 2020). Interestingly, differential gene expression in post-mortem brains with Braak scores of 1-2, 3-4, and 5-6 and controls, suggested a role for oligodendrocytes at an early stage of PD prior to the overt loss of dopaminergic neurons (Bryois et al., 2020). Additionally, two independent single-cell sequencing studies, one of the human substantia nigra and one of the midbrain, both associated PD genetic risk with oligodendrocyte-specific expression patterns (Agarwal et al., 2020; Smajic et al., 2022). While these studies started to link dysfunction of oligodendrocytes to the early stages of PD, they did not address their role in the pathophysiology of the disease.

Here, we describe a *Drosophila* model to start assessing how neuron-glia cross-talk contributes to PD. *Drosophila* has been successfully used to investigate cellular and molecular dysfunction preceding the onset of age-related symptoms, including dopaminergic neuron-dependent motor symptoms (Kaempf et al., 2026; Pech et al., 2025; Valadas et al., 2018). Furthermore, *Drosophila* glial cells display several anatomical and functional features that show remarkable similarity to their mammalian counterparts (Freeman & Doherty, 2006; Kremer et al., 2017). While the small size of the *Drosophila* brain does not necessitate elaborate myelination, ensheathing glia (EG) in this species share not only anatomical features with oligodendrocytes, such as the ability to wrap around nerve tracts in the Central Nervous System (CNS) (Kremer et al., 2017; Yildirim et al., 2019), but also important molecular and functional features, such as providing metabolic support and regulating neuronal activity (Delgado et al., 2018; Otto et al., 2018).

In a brain-wide single-cell sequencing experiment, we identified EG as the most deregulated cell type in a young (pre-motor) *Pink1* loss-of-function *Drosophila* model. Using cell-specific labeling, immunohistochemistry, and electrophysiological recordings, we correlated the transcriptional deregulation in EG with defects that appear similar to those seen upon nerve injury. Additionally, we find that healthy EG are fundamental to support dopaminergic synapse integrity in *Pink1* mutants. Finally, using cell-type-specific transcriptomic, high-throughput screening and immunohistochemistry, we identified vesicle trafficking as a genetic modifier and showed that *Vps13* and *Vps35* are EG-expressed regulators that maintain dopaminergic synapse integrity. Our study shows that neuron-ensheathing glia crosstalk is already disrupted at a young age by the loss of *Pink1* in neurons, but also in EG, and that EG are fundamental to support dopaminergic synapse-integrity, suggesting a role for oligodendrocytes in the progression of PD.

Results

Ensheathing glia in Pink1 loss-of-function flies show cell non-autonomous defects

We previously created a whole-brain single-cell RNAseq dataset from different *Drosophila* PD knock-in models. This dataset was generated from young 5-day-old flies to capture 'early' changes (Pech et al., 2025). We re-analyzed the data from $Pink1^{P399L}$ knock-in loss-of-function mutant flies and isogenic controls and performed differential gene expression (DEG) analysis for each cell type using DESeq2 (Figure 1A). Glial cell subtypes show the highest degree of deregulation; particularly, ensheathing glia are strongly affected (Figure 1A). While flies do not myelinate neurons, ensheathing glia (EG) serve similar supporting functions as oligodendrocytes (Otto et al.,

2018; Yildirim et al., 2019). These results suggest that ensheathing glia are deregulated in young *Pink1*^{P399L} mutants (and also *Pink1*$^{KO\text{-}WS}$, see below) at an age prior to dopaminergic neuron-dependent motor defects (Kaempf et al., 2026; Pech et al., 2025).

When neurons are damaged, activated EG invade the neuropil (Doherty et al., 2009; MacDonald et al., 2006). For example, when fly antennal lobes are removed, severing the Olfactory Receptor Neurons (ORNs), EG invade the antennal lobe neuropil (MacDonald et al., 2006), potentially as a protective response (Figure 1B'-C). To test if EG invaded the neuropil in *Pink1* mutant flies, we expressed a transmembrane fluorescent protein (*UAS-CD8GFP*) under the control of a promoter specific to EG (*MZ709-Gal4*) (Doherty et al., 2009, Supplementary figure 1) in control and *Pink1*^{KO} flies. Samples were labeled with anti-GFP and the pre-synaptic protein Bruchpilot (NC82). Similar to ORN-severed controls, GFP signal, lining the membrane of EG, is visible inside the antennal neuropil in *Pink1*^{KO}, and severing the ORN in *Pink1*^{KO} does not further exacerbate this phenotype (Figure 1B"-C). Even though we cannot exclude that in *Pink1* mutants the GFP signal is merely upregulated, *Pink1* loss and neuron-severing that triggers EG activation seem to have a similar phenotype.

In order to determine whether this phenotype is cell-autonomous, we generated cell-type-specific *Pink1* perturbations. We either downregulated *Pink1* using a previously well-validated RNAi line specifically in EG (EG-specific *Pink1* loss-of-function – Figure 1D'), or we re-expressed wild-type *Pink1* specifically in EG in *Pink1*$^{KO\text{-}WS}$ flies (all cells, but the EG, loss-of-function - Figure 1D"). When *Pink1* is knocked-down in EG (but present in other cells, including neurons), no GFP signal is detected in the neuropil (Figure 1D''-1E). However, when *Pink1* is not present in neurons and expressed in EG, the GFP is present inside the antennal neuropil (Figure 1D"-E). This suggests that Pink1-defective neurons activate the EG in a cell-nonautonomous fashion to invade, and potentially protect, the neuropil.

Ensheathing glia function supports synaptic integrity

Our finding that *Pink1*$^{KO\text{-}WS}$ in neurons elicits a cell non-autonomous response in EG suggested that EG might, in turn, also functionally modulate neuronal integrity in mutant flies. To test this, we made use of a readily accessible model circuit in the fly visual system with an easy electrophysiological read-out, electroretinograms (ERG). Notably, whereas our functional readout here interrogates neuronal activity in the visual system, our analysis of EG morphology was performed in the antennal lobe, a distinct brain region. We therefore make the explicit assumption that EG perform comparable functions across fly brain regions. This assumption is supported by our single-cell sequencing dataset, in which we did not detect region-specific segregation of EG into distinct clusters that could be attributed to different brain areas. The ERG waveforms are susceptible to changes in intracellular signaling, neuronal function, and synaptic transmission, and have been well characterized and amply used to assess neuronal and cellular function (Hardie & Raghu, 2001; Praschberger et al., 2023; Soukup et al., 2016; C. F. Wu & Wong, 1977). We exploited this method to understand the role of *Pink1* in EG on neuronal function and synaptic transmission in young flies.

Comparing control with young *Pink1*$^{KO\text{-}WS}$ flies does not show a difference in the "depolarization-response", indicating that -as expected-there is no neurodegeneration occurring in the photoreceptors at this stage (Figure 2A). However, when comparing the ON peak – which represents synaptic transmission from the photoreceptors and within the underlying neuronal circuit, and is a more robust readout of this than the OFF peak (Vilinsky & Johnson, 2012) – we detect a significant reduction in mutant compared to control animals, suggesting that in *Pink1*$^{KO\text{-}WS}$ flies, synaptic communication in this circuit is partially impaired, already at 5-day-old (Figure 2A-B).

In order to discern the role of EG in this defective ERG response, we (1) downregulated *Pink1* specifically in EG and (2) we expressed *Pink1* specifically in the EG of *Pink1*$^{KO\text{-}WS}$. When *Pink1* is knocked down specifically in EG, we observe the same reduction in ON peak response as in the *Pink1*$^{KO\text{-}WS}$ flies. This indicates that EG integrity is necessary for efficient neurotransmission in

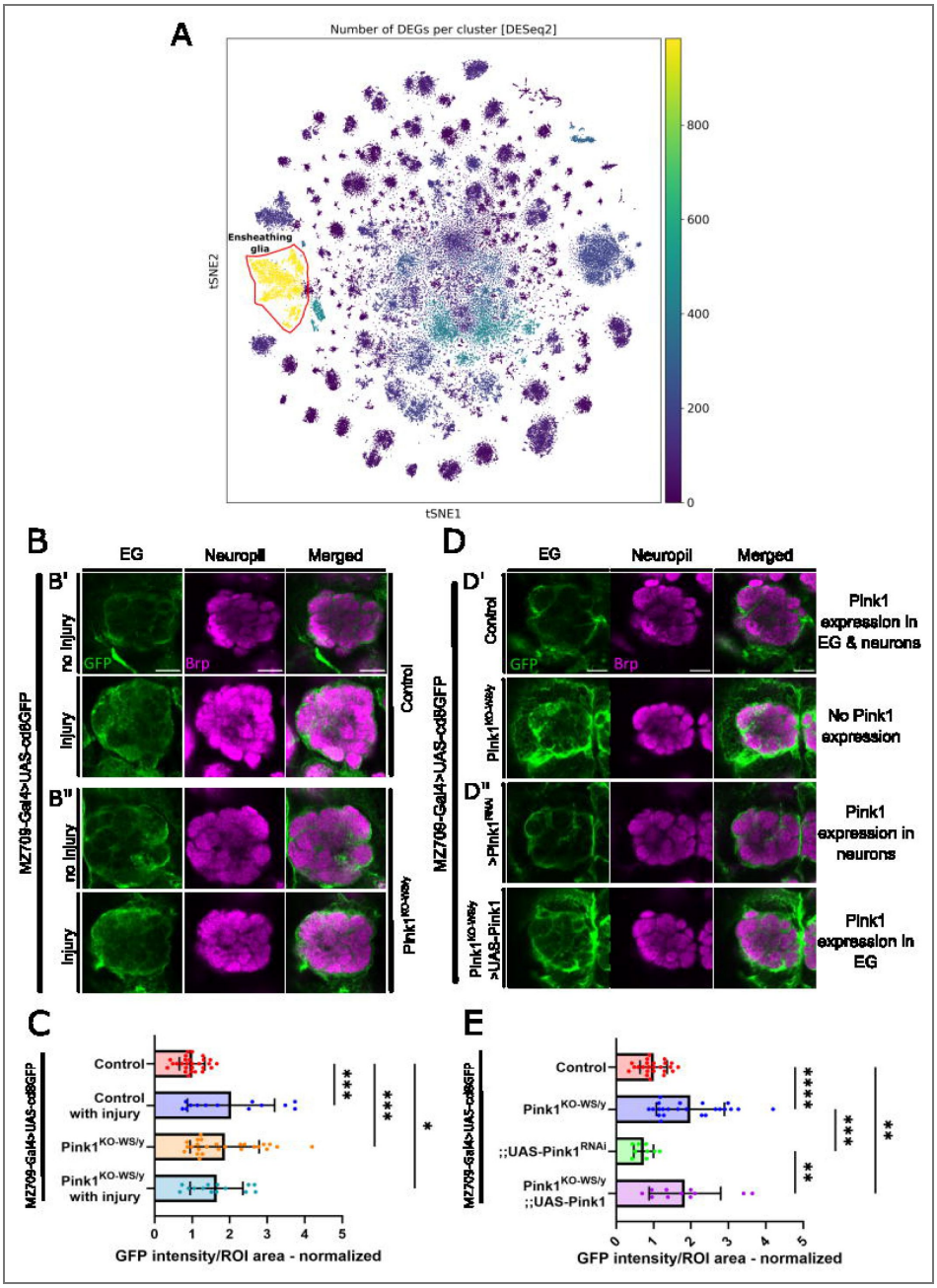

Figure 1. EG are affected non-cell autonomously by *Pink1* loss-of-function (with supplementary fig 1)

(A) tSNE of the cells of *Pink1*^{P399L} knock-in mutants (5-day-old). Cell types are labeled with colors indicating the number of deregulated genes compared to control. EG are encircled and labeled. (**B-B"**) Maximum intensity projections of confocal images of fly brains (5 ± 1-day-old) stained with anti-GFP (Green) and anti-Brp (Magenta), where anti-GFP marks EG and anti-Brp marks presynaptic sites of the antennal lobes in flies where CD8GFP is expressed via the EG driver MZ709-Gal4. Scale bar: 20 µm (**B'**) Maximum intensity projection of confocal images of controls vs. controls 24 hours after ORN-severing (injury). (**B"**) Maximum intensity projection of confocal images of *Pink1*$^{KO\text{-}WS}$ vs *Pink1*$^{KO\text{-}WS}$ 24 hours after ORNs severing (injury). (**C**) Quantification of GFP intensity within the glomeruli of the antennal lobe area in 5 ± 1-day-old flies (as in B) relative to controls. ANOVA with Dunnet's multiple comparison test, * is p<0.05, ** is p<0.01, *** is p<0.001. Effect size: η =0.23. Bars: mean ± SD; points are individual animals N≥13 per genotype, 4 replicates. (**D-D"**) Maximum intensity projection of confocal images of fly brains (5 ± 1-day-old) stained with anti-GFP (Green) and anti-Brp (Magenta), where anti-GFP marks EG and anti-Brp marks presynaptic sites of the antennal lobes in flies where CD8GFP is expressed via the EG driver MZ709-Gal4. Scale bar: 20 µm. (**D'**) Maximum intensity projection of confocal images of control (*w*^{1118}) and *Pink1*$^{KO\text{-}WS}$ animals (**D"**) Maximum intensity projection of confocal images of animals with *Pink1* downregulation in EG and *Pink1*$^{KO\text{-}WS}$ with *Pink1* rescued in EG. (**E**) Quantification of GFP intensity within the glomeruli of the antennal lobe area in 5-day-old flies (as in D) relative to the control. ANOVA with Tukey's multiple comparison test, * is p<0.05, ** is p<0.01, *** is p<0.001. Effect size: η =0.36 Bars: mean ± SD; points are individual animals N≥10 per genotype, 4 replicates.

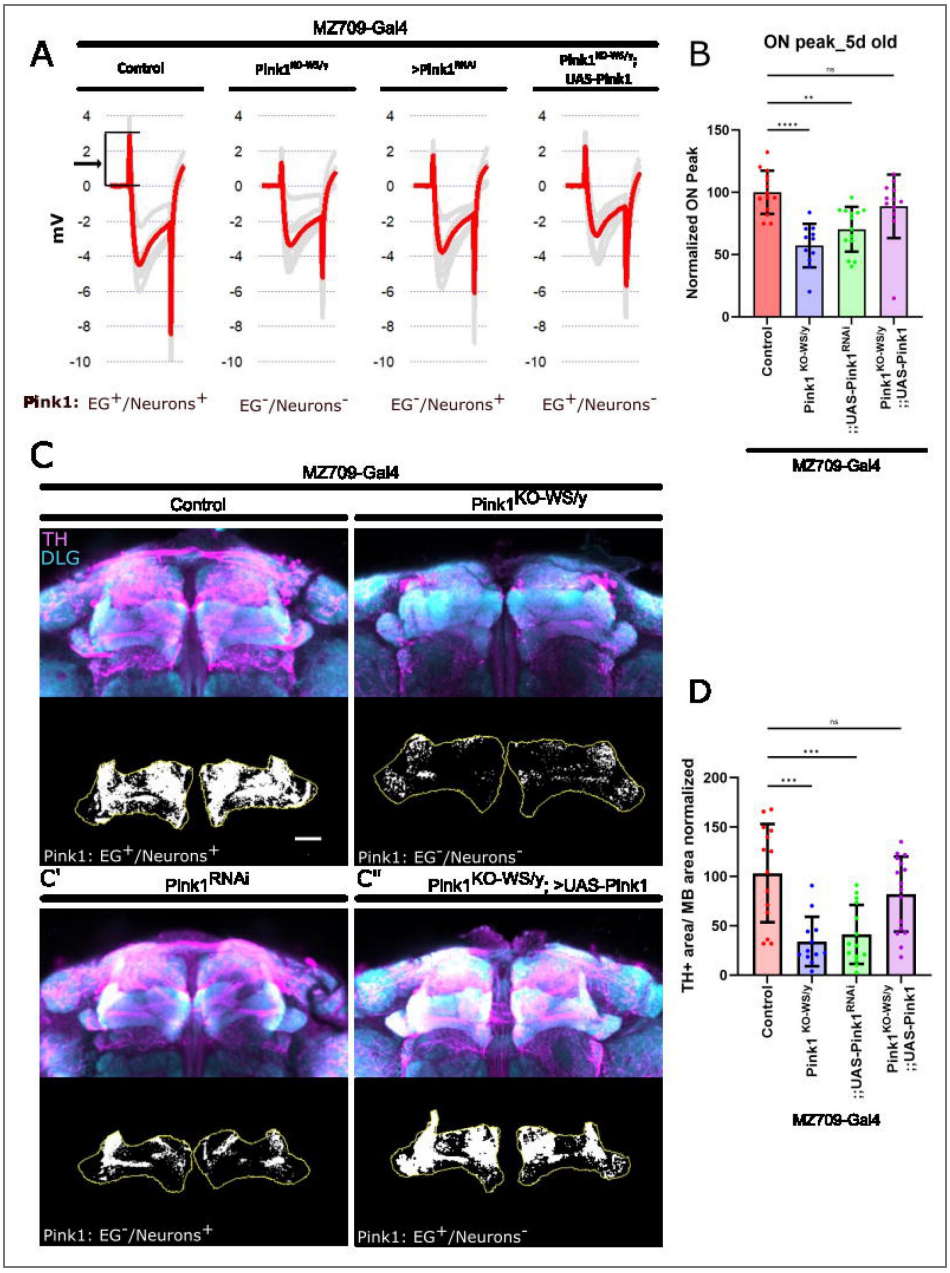

Figure 2. ***Pink1*** **in EG is necessary to support synaptic integrity (with Supplementary figure 2)**

(**A**) Representative ERG traces of indicated genotypes: ON peak is highlighted by the arrow. (**B**) Normalized ON peak amplitude of flies (5 ± 1-day-old). ANOVA with Tukey's multiple comparison test, * is p<0.05, ** is p<0.01, *** is p<0.001. Effect size: η =0.55 Bars: mean ± SD; points are individual animals N≥11 per genotype, 3 replicates. (**C-C"**) (**C**) Maximum intensity projection of confocal images of control and *Pink1*$^{KO-WS}$ in Mushroom Bodies (MB) of aged flies (22 ± 2-day-old), stained with anti-TH (cyan) and anti-DLG (magenta) antibodies - DLG is used to mark post-synaptic sites of MB. The black and white image is the middle Z-plane within the region of interest of the MB (ROI, yellow), which is used to represent the thresholded TH area (white). Scale bar: 20 µm. (**C'**) Maximum intensity projection of confocal images of *w*^{1118} with *Pink1* downregulation in EG. (**C"**) Maximum intensity projection of confocal images of *Pink1*$^{KO-WS}$ with *Pink1* rescued in EG. (**D**) Quantification of the dopaminergic synaptic area at MB neuropil in aged flies (22 ± 2-day-old). ANOVA with Tukey's multiple comparison test, * is p<0.05, ** is p<0.01, *** is p<0.001. Effect size: η = 0.38. Bars: mean ± SD; points are individual animals N≥12 per genotype, 3 replicates.

this circuit. Conversely, the ON peak defect of *Pink1*$^{KO\text{-}WS}$ mutants is rescued when *Pink1* is reintroduced in EG only. This suggests that activated EG are able to, at least partially, buffer the detrimental effects of *Pink1* deficiency in neurons (Figure 2A-B).

To also test EG function in relation to PD-relevant dopaminergic (DA) synapses, we evaluated the loss of dopaminergic neuron afferents. In a previous paper from our laboratory, we have shown that the loss of *Pink1* function causes a progressive loss of protocerebral anterior medial dopaminergic neuron (PAM DAN) afferents in the Mushroom Body (MB) neuropil in 25-day-old animals, but not when they are 5-day-old (Kaempf et al., 2026). Indeed, we confirm that 25-day-old animals show a decrease in the dopaminergic synaptic area in MB lobes (Figure 2 C-D). Hence, while ensheathing glia are already activated at a young age in *Pink1*$^{KO\text{-}WS}$, DA synapses are structurally still intact (at 5 days of age) and only deteriorate in older flies. We then knocked down *Pink1* specifically in EG and found a similar strong decrease in DA synaptic area (Figure 2C'-D). Conversely, when *Pink1* is reintroduced specifically in EG of *Pink1*$^{KO\text{-}WS}$ animals, DA synapse-loss is significantly rescued (Figure 2C"-D and Supplementary figure 2). Together, these results indicate that *Pink1* in EG is necessary to protect dopaminergic neurons from synapse loss.

EG cell type-specific transcriptomics reveals modifiers of neuronal dysfunction

To identify pathways in EG that are deregulated by *Pink1* loss-of-function, we optimized a method to isolate EGs from the rest of the brain, enabling us to perform much higher-sensitivity transcriptomics than what we achieved with our 10x droplet-based single-cell sequencing (Pech et al., 2025). We expressed a fluorescently-tagged histone (*UAS-HisTag-eGFP*) in EG (GMR-56-Gal4) and used Fluorescence-activated Cell Sorting (FACS) to isolate EG. We sorted 300 cells per technical replicate and performed Bulk-RNA sequencing using a SMART-seq2 protocol (Figure 3A). The sequencing results of EG-sorted cells and of neuron-sorted cells (*nSyb-Gal4* instead of *GMR-56-Gal4*) show strong enrichment of EG cell markers in the former and strong enrichment of neuronal markers in the latter (Figure 3B). We then compared the transcriptomic profile of EG in *Pink1*$^{KO\text{-}WS}$ to that of control using differential expression analysis and found 617 deregulated genes in EG (Appendix 1, padj<0.05) (Figure 3C). To understand whether the deregulated genes were enriched for a specific pathway or associated with a cellular component compared to non-significantly deregulated genes, we performed Gene Ontology analysis of the deregulated genes in *Pink1*$^{KO\text{-}WS}$ flies. Our analysis resulted in generic terms and very diverse pathways that did not allow us to draw further conclusions.

To test if the genes deregulated in EG are modifiers of the neuronal *pink1*$^{KO\text{-}WS}$ phenotypes, we downregulated and upregulated (when possible) the 50 most deregulated genes (Figure 3C), for which we could find RNAi fly lines, specifically in the EG of *Pink1*$^{KO\text{-}WS}$ flies and recorded ERGs in 5-day-old animals. Knock down of one of the genes (*CG17660*) resulted in a rescue of the ON transient defects in *Pink1*$^{KO\text{-}WS}$ (suppressors at p<0.05), and a few exacerbated the defect (Figure 3D). Interestingly, the human orthologs of *CG17660, TMEM87A/B*, have an established role in endosomal sorting (Gaudet et al., 2011; Hirata et al., 2015). Hence, our genetic screening suggests that *Pink1*$^{KO\text{-}WS}$ phenotypes might be suppressed by downregulating genes involved in vesicle trafficking in EG.

PD causative vesicle trafficking gene downregulation in EG rescues synaptic dopaminergic neurons afferent loss

Because our ERG-based modifier screen for the *Pink1*$^{KO\text{-}WS}$ phenotype identified a gene with a known role in vesicle trafficking, we next asked whether *Pink1* in EG also genetically interacts with other PD-causative genes that function in vesicle trafficking, specifically vesicle trafficking components affecting membrane interactions between mitochondria and the endoplasmic reticulum (ER), like *Vps35* and *Vps13* (Brickner & Fuller, 1997; Lesage et al., 2016; Vilariño-Güell et al., 2011; Zimprich et al., 2011). We find that the knock down of each of these genes in EG also rescues the ON transient defect of *Pink1*$^{KO\text{-}WS}$ mutants (Figure 4A-B).

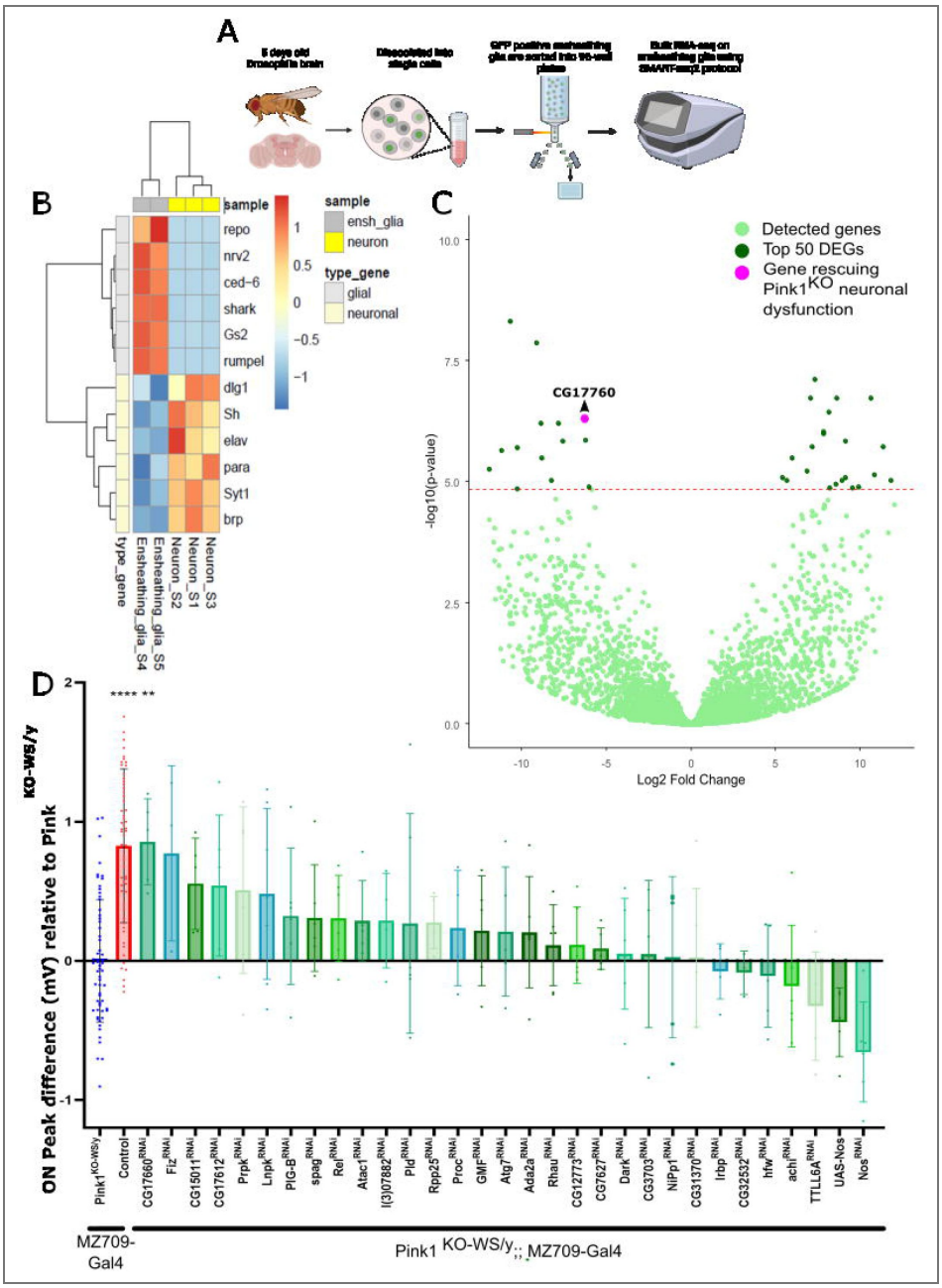

Figure 3. **Cell type-specific transcriptomics reveals modifiers of neuronal dysfunction**

(**A**)Scheme of cell-type specific transcriptomics (created using *BioRender.com*). (**B**)Scaled gene expression of representative genes for EG and neurons after sorting EG or neurons using the protocol described in (A) (R Core Team, 2022). N=2, 2 replicates. (**C**)Differentially expressed genes in EG in *Pink1*$^{KO\text{-}WS}$ compared to control flies, plotted according to their Log2 Fold change and the -Log10 of the adjusted p-value. Intercept in red (-Log10 adjusted p-value = 4.31); light green dots are all detected genes, dark green are the 50 most deregulated genes, and the pink dot is from a gene positive in the genetic screen (D). *Two data points are outside the boundaries of the plot. To determine the transcriptomic profile of each genotype, a N=3 was used, and 3 replicates were performed. (**D**)ERG ON peak value differences to *Pink1*$^{KO\text{-}WS}$ flies (5 ± 1-day-old) of control (red) and of *Pink1*$^{KO\text{-}WS}$ flies with DEGs downregulated, or upregulated, specifically in EG (5 ± 1 days old). ON peak values are expressed as the difference to *Pink1*$^{KO\text{-}WS}$. ANOVA with Dunnett's test, * is p<0.05, ** is p<0.01, *** is p<0.001. Effect size: η = 0.44. Bars: mean ± SD; points are individual animals N≥3 per genotype. *One data point is outside the boundaries of the plot.

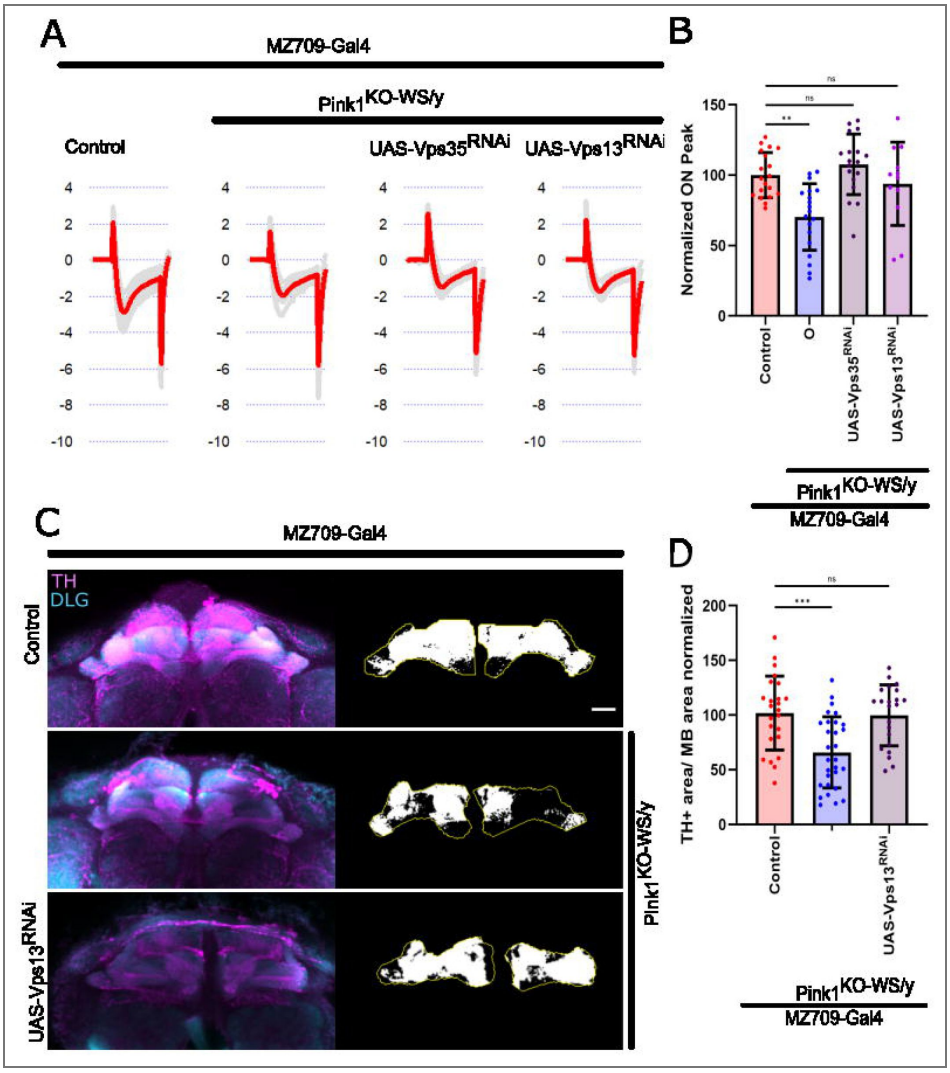

Figure 4. ***Vps35*** **and** ***Vps13*** **downregulation in EG rescues synaptic deficits in** ***Pink1^{KO-WS}*** **flies (with supplementary figure 3)**

(**A**)Representative ERG traces of control,*Pink1^{KO-WS}* flies and *Pink1^{KO-WS}* flies with *Vps35* or *Vps13* downregulated in EG. (**B**)Quantification of the normalized ON peak response of flies with the genotypes in (A) (5 ±1-day-old). ANOVA with Dunnett's multiple comparison test, * is p<0.05, ** is p<0.01, *** is p<0.001. Effect size: η = 0.48. Bars: mean ± SD; points are individual animals N≥10 per genotype, 3 replicates. (**C**)Maximum intensity projection of confocal images of Mushroom Bodies (MB) of aged flies (22 ± 2-day-old) of control, *Pink1^{KO-WS}* flies and *Pink1^{KO-WS}* flies with *Vps13* downregulated in EG, labeled with anti-TH (cyan) and anti-DLG (magenta), DLG is used to mark the MB neuropil. The black and white image is the middle Z-plane within the region of interest of the MB (ROI, yellow), which is used to represent the thresholded TH area (white). Scale bar: 20 μm. (**D**)Quantification of the dopaminergic synaptic area within MB of aged flies (22 ± 2-day-old). ANOVA with Dunnett's multiple comparison test, * is p<0.05, ** is p<0.01, *** is p<0.001. Effect size: η =0.23. Bars: mean ± SD; points are individual animals n≥22 per genotype, 5 replicates.

To determine if manipulation of this pathway in EG can also rescue the synaptic innervation defect of PAM DAN onto the mushroom bodies in old (20-25-day-old) *Pink1*$^{KO-WS}$ mutants, we expressed RNAi to *Vps13* in EG using *MZ709-Gal4*. Anti-TH labeling (marking DAN synapses) in the MB area (marked by anti-DLG) is significantly reduced in aged *Pink1*$^{KO-WS}$, but is rescued to control levels when *Vps13* is knocked down in EG (Figure 4C-D, Supplementary figure 3). These results suggest that manipulation of vesicle trafficking components affecting membrane interactions between mitochondria and the ER in EG regulate glia-neuron crosstalk to maintain synaptic integrity of dopaminergic neuron synapses in the fly brain of *Pink1* mutants.

Discussion

In this work, we provide evidence for early, non-cell-autonomous activation of EG in a PD-relevant *Drosophila Pink1* model. This occurs already in young *Pink1*-mutant flies when neuronal defects in dopaminergic neurons are not yet measurable. The EG activation and invasion phenotype appears as a protective response, as Pink1-deficient neurons seem to show defects in EG that mimic the response to nerve injury (Doherty et al., 2009; MacDonald et al., 2006). In addition to this, we show that there is also a non-autonomous role of EG to support *Pink1*-deficient neurons. When we manipulate the expression of membrane-lipid trafficking genes, the homologs of the established PD genes VPS13C and VPS35 (Lesage et al., 2016; Vilariño-Güell et al., 2011; Zimprich et al., 2011), specifically in EG, we rescue the dysfunction of *Pink1* mutant neuron defects (ERG and PAM DAN synapse loss). Our work shows the importance of neuron-glia cross-talk in the context of Pink1-deficiency. We suggest (1) there is early EG activation secondary to *Pink1*-loss-induced neuronal impairments; (2) there are specific lipid- and membrane trafficking problems caused by *Pink1* loss in EG that center on mitochondria/ER contacts and (3) there is a convergence of Parkinson-relevant genetic factors that act in EG to maintain neuronal function.

The loss of Pink1 function in the context of Parkinson's disease has been amply linked to the regulation of mitochondrial health. Pink1 maintains the integrity of the electron transport chain by phosphorylating NDUFA10 (Morais et al., 2009, 2014; Pogson et al., 2014) and when mitochondria are damaged, it phosphorylates Parkin and Ubiquitin to facilitate mitophagy (Kane et al., 2014; Narendra et al., 2010; Narendra & Youle, 2024). The regulation of mitophagy is complex and requires mitochondrial rearrangements controlled by mitochondria-organelle contacts (ER and lysosomes) (Wong et al., 2018, 2019; Yamano et al., 2018). Such contacts mediate inter-organellar lipid exchange as well as facilitate organellar fusion (Kumar et al., 2018; Valadas et al., 2018). In *Pink1* mutants, these contacts appear to be increased in number, and this causes cellular defects (Grossmann et al., 2023; Valadas et al., 2018).

We found that in EG, *Vps35* functionally interacts with Pink1-induced neuronal dysfunction: its genetic manipulation in EG rescues cell non-autonomous neuronal dysfunction. Loss of *Vps35* itself only in EG is sufficient to rescue neuronal *Pink1* phenotypes. *Pink1* loss-of-function models show increased numbers of mitochondria-ER contact sites (Valadas et al., 2018), affecting mitochondrial calcium levels (Barazzuol et al., 2020; De Brito & Scorrano, 2008; Ham et al., 2023) and dysregulating lipidic ER composition (Valadas et al., 2018) (Figure 5A). Indeed, *Pink1* is necessary for ubiquitination and degradation of Mitofusin (Poole et al., 2010), which is fundamental for the mitochondria-ER tethering (De Brito & Scorrano, 2008). Interestingly, *Vps35* deficiency promotes untethering of mitochondria-ER contact sites by increasing the mitochondrial levels of MUL1, which is necessary for the ubiquitination and degradation of Mitofusin (Puri et al., 2019; Tang et al., 2015; Yun et al., 2014). Hence, conditions that affect mitochondria-ER contact site regulation in EG, by modifying an endosomal trafficking regulator such as *Vps35*, are expected to rescue *Pink1* neuronal dysfunction, possibly by restoring mitochondrial calcium levels and the lipid composition of the ER (Figure 5B); but further work is needed to sort these mechanistic elements in a cell-specific manner.

Our observation that downregulation of *Vps13* in EG also rescues *Pink1* is in further support of a role for ER-mitochondria contact site regulation. *Vps13* has two mammalian homologs, VPS13A and VPS13C (Velayos-Baeza et al., 2004; Vonk et al., 2017; Vrijsen et al., 2022), which are also mutated in familial Parkinsonism/neurodegenerative disease (Lesage et al., 2016). VPS13A

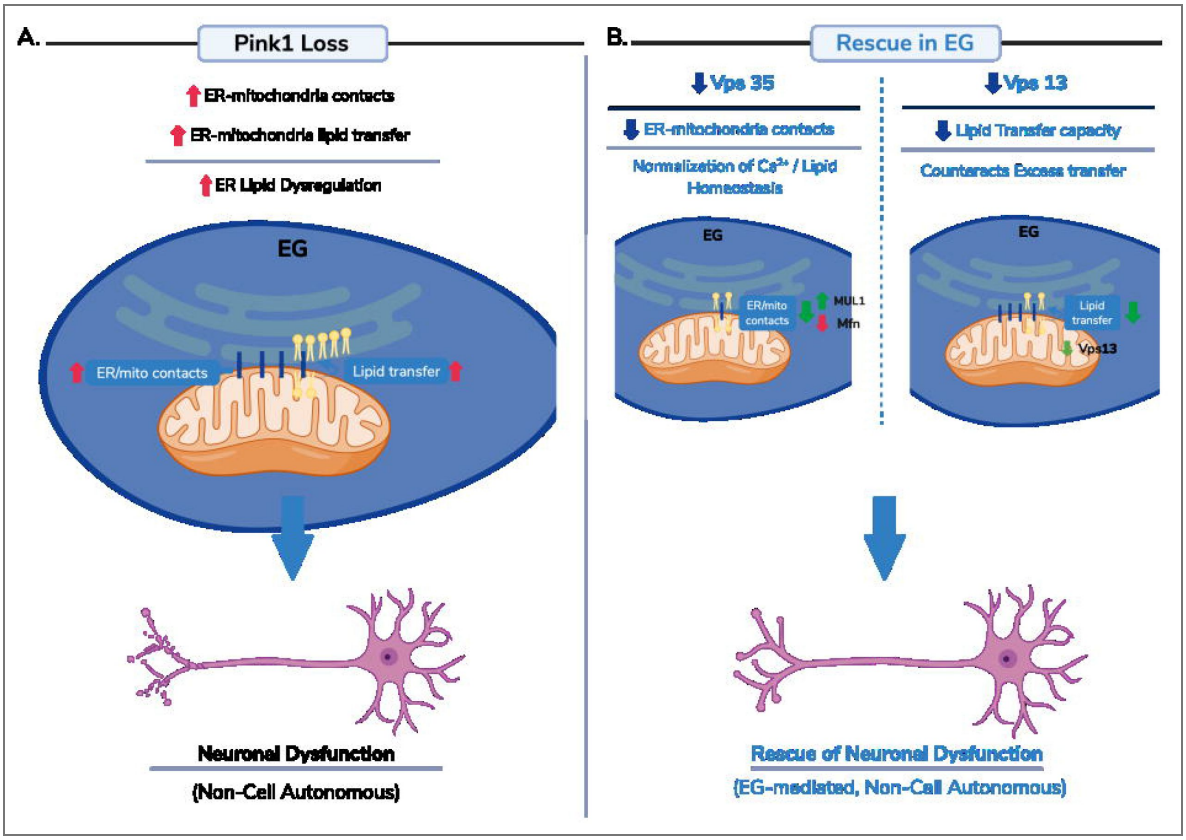

Figure 5. Modulation of ER–mitochondria contact sites and lipid transfer in ensheathing glia (EG) rescues Pink1-dependent neuronal dysfunction.

Schematic representation of the suggested model (created using *BioRender.com*). (A)Loss of *Pink1* leads to an abnormal increase in endoplasmic reticulum (ER)–mitochondria contact sites (represented by blue thick lines), resulting in enhanced ER-to-mitochondria lipid transfer and dysregulation of ER lipid composition (represented by yellow lipids). Increased organelle membrane contacts and lipid flux in EG contribute to neuronal dysfunction in a non–cell autonomous manner. (B)Genetic downregulation of ER–mitochondria contact and lipid transfer regulators in EG rescues Pink1-induced neuronal phenotypes through two convergent mechanisms. Reduction of Vps35 decreases the number of ER–mitochondria contact sites, likely via MUL1-mediated Mitofusin (Mfn) turnover, leading to normalization of calcium and lipid homeostasis. In parallel, downregulation of Vps13, a lipid transfer facilitator at organelle contact sites, limits ER-to-mitochondria lipid transfer capacity, counteracting the excessive lipid flux induced by Pink1 loss. Both interventions restore organelle homeostasis in EG and result in rescue of neuronal dysfunction through a non–cell autonomous mechanism.

tethers ER to mitochondria and lipid droplets, and VPS13C tethers ER to late endosomes, lysosomes and lipid droplets (Kumar et al., 2018; Muñoz-Braceras et al., 2019; Vrijsen et al., 2022). The function of these proteins is to facilitate lipid transfer between organelles, a function we previously showed to be increased in *Pink1* mutants (Valadas et al., 2018). Hence, the downregulation of *Vps13* would counteract the effects of excessive organelle membrane contact formation and dysregulated lipid homeostasis in *Pink1* mutants (Figure 5B).

Lipid homeostasis in glial cells is crucial for supporting neuronal function by providing energy, protecting against oxidative stress, and regulating synaptic health. In oligodendrocytes, maintaining myelin sheaths is critical (Ettle et al., 2016; Lappe-Siefke et al., 2003). While fly EG do not generate such structures, they do wrap processes around neuropil regions, also requiring lipid membrane production (Kremer et al., 2017; Pogodalla et al., 2021). Through lipid metabolism, glia also supply neurons with essential metabolites, cholesterol, and signaling molecules that aid in membrane integrity, synaptic remodeling, and neuroprotection (Delgado et al., 2018; Otto et al., 2018; Saab et al., 2016; Suárez-Pozos et al., 2020). Further work is now required to define which functions, supported by organelle contact sites in glial cells, drive cell-nonautonomous protective mechanisms in neurons. Our work in flies indicates these glial defects precede dopaminergic synapse loss, and, importantly, that rescuing the glial defects helps to prevent dopaminergic problems later in life.

Methods

Resource availability

Lead Contact

Further information and requests for resources and reagents should be directed to the lead contact, Patrik Verstreken (*patrik.verstreken@kuleuven.be*).

Materials Availability

Data, code, Drosophila models, and reagents are available upon request.

Fly stocks

The fruit flies were maintained in an incubator at 25°C under a 12h:12h light-dark cycle and provided with a standard diet consisting of corn meal and molasses. For experiments, only male flies were used. Flies were raised in parallel on the same batch of food, which was exchanged every three to four days and kept in only male population of similar density. Flies were aged to 5 ± 1-day-old, and 22 ± 2-day-old, as indicated for immunohistochemistry and ERGs, respectively.

To create a set of *Drosophila* models for Parkinson's disease, CRISPR/Cas9-based gene editing was utilized, as outlined in (Kaempf et al., 2026; Pech et al., 2025). In brief, each knock-out line contained an attP-flanked w+ reporter cassette that replaced the first shared exon across different isoforms of the targeted gene. For this study, we used knockout flies for *Pink1* from this collection (Kaempf et al., 2026). The "control" strain denotes a semi-isogenized w^{1118} strain that underwent backcrossing to Canton-S for 10 successive generations, resulting in a strain termed Canton-S-w1118. To generate the fly line *yw; UAS-His2Av::eGFP.VK27/TM3Sb*, we created the pUASTattB_His2AV-GFP plasmid, linearizing the pUAST.attB (Bischof et al., 2007) with EcoRI-BamHI. A gBlock, containing the His2AV, GS linker and eGFP sequence, was cloned into this linearized plasmid with Gibson Assembly. The plasmid was inserted into the VK27 landing site by BestGene. The sequence His2AV-GS-eGFP gblock is:

TGAATAGGGAATTGGGcAAacATGGCTGGCGGTAAAGCAGGCAAGGATTCGGGCAAGGCCAAGGCGAAGG
C GGTATCGCGTTCCGCGCGCGCGGGTCTTCAGTTCCCCGTGGGTCGCATCCATCGTCATCTCAAGAGCCGCA
CTA CGTCACATGGACGCGTCGGAGCCACTGCAGCCGTGTACTCCGCTGCCATATTGGAATACCTGACCGCCG
AGGT CCTGGAGTTGGCAGGCAACGCATCGAAGGACTTGAAAGTGAAACGTATCACTCCTCGCCACTTACAG
CTCGCC ATTCGCGGAGACGAGGAGCTGGACAGCCTGATCAAGGCAACCATCGCTGGTGGCGGTGTCATTCC
GCACATA CACAAGTCGCTGATCGGCAAAAAGGAGGAAACGGTGCAGGAcCCGCAGCGGAAGGGCAACGTC
ATTCTGTCG

AGGAGCTGTT CACCGGGGTGGTGCCCATCCTGGTCGAGCTGGACGGCGACGTAAACGGCCACAAGTTCAGC GTGTCCGGCGA GGGCGAGGGCGATGCCACCTACGGCAAGCTGACCCTGAAGTTCATCTGCACCACCGGCAA GCTGCCCGTGCC CTGGCCCACCCTCGTGACCACCCTGACCTACGGCGTGCAGTGCTTCAGCCGCTACCCCGA CCACATGAAGCAG CACGACTTCTTCAAGTCCGCCATGCCCGAAGGCTACGTCCAGGAGCGCACCATCTTCTT CAAGGACGACGGCA ACTACAAGACCCGCGCCGAGGTGAAGTTCGAGGGCGACACCCTGGTGAACCGCATC GAGCTGAAGGGCATCG ACTTCAAGGAGGACGGCAACATCCTGGGGCACAAGCTGGAGTACAACTACAACA GCCACAACGTCTATATCAT GGCCGACAAGCAGAAGAACGGCATCAAGGTGAACTTCAAGATCCGCCACAAC ATCGAGGACGGCAGCGTGCA GCTCGCCGACCACTACCAGCAGAACACCCCCATCGGCGACGGCCCCGTGCT GCTGCCCGACAACCACTACCTG AGCACCCAGTCCGCCCTGAGCAAAGACCCCAACGAGAAGCGCGATCACA TGGTCCTGCTGGAGTTCGTGACCG CCGCCGGGATCACTCTCGGCATGGACGAGCTGTACAAATAAGGGTAC CTCTAGAGGATCTT.

Flies were backcrossed for five generations into an inbred Canton-S strain harboring the w^{1118} mutation. The genotypes used in this study are listed in the key resource table and Supplementary table 1.

Olfactory Receptor Neurons (ORNs) axotomy

ORN bilateral axotomy was performed on 4±1 day old flies by surgical ablation of the third antennal segment. Briefly, flies were anesthetized with CO_2, and then both antennae were removed with Dumont #5 forceps and returned to the vial (M. Purice, 2020; M. D. Purice et al., 2017). Flies recovered for 24 h on food at 25°C before dissection.

Immunohistochemistry and confocal imaging – invasion phenotype

Immunohistochemistry was performed on adult fly brains of 5±1-day-old, with at least two independent experiments. The brains were dissected in ice-cold PBS and fixed for 20 min in freshly prepared 3.7% paraformaldehyde (in 1x PBS, 0.3% Triton X-100 [PBX] [Sigma]) at room temperature (RT), followed by three 15-min washes in PBX at RT on a shaker. Then, the brains were incubated for 1 h in blocking solution (PBX, 10% normal goat serum [NGS]) at RT. Following blocking, the brains were incubated with primary antibodies (rabbit anti-GFP [Thermo Fisher Scientific], 1:1000, mouse anti-brp [DSHB, nc82], 1:100) in blocking solution at 4°C overnight, followed by three 15-min washes in PBX at RT. Secondary antibodies (goat anti-rabbit Alexa488, goat anti-mouse Alexa555, both at 1:1000 [Thermo Fisher Scientific]) in PBX with 10% NGS were applied overnight at 4°C. Afterwards, the brains were washed three times for 15 min in PBT at RT on a shaker and mounted with the anterior facing up in RapiClear 1.47 (SUNJin Lab). Imaging was performed using a Nikon A1R confocal microscope with a 40x (NA 1.15) water immersion lens; Z-stacks of the entire antennal lobes were acquired. The acquisition was carried out using a Galvano scanner, with a zoom factor of 1, scan speed of 0.5, and line averaging set to 2. All images were captured with a pinhole of 0.9 Airy units and a resolution of 1024 × 1024. Z-stacks (with 0,5 µm step intervals) were obtained for data acquisition, and the same imaging settings were applied across all genotypes and sessions. Image analysis was performed using Fiji (Schindelin et al., 2009). Image analysis was performed using Fiji (Schindelin et al., 2009). Each antennal lobe is composed of multiple glomeruli, and EG separate them and invade them when active (Doherty et al., 2009; Pogodalla et al., 2021). To quantify EG invasion in the antennal lobe, we calculated the invasion in every single glomerulus. To do so and be consistent with the section of the antennal lobe analyzed, anti-brp was used to identify the 3 Z-planes where DM6 and DM1 glomeruli were present (B. Wu et al., 2017). Then, to automatically detect and segment each glomerulus of the antennal lobe section, regions of interest (ROIs) were defined in the SUM projection of the 3 Z-planes by using the Fiji plugin Stardist (Weigert et al., 2019).

To quantify the EG invasion in the ROIs, anti-GFP SUM projection of the same 3 Z-planes was used. The GFP intensity was detected in each ROI, and it was normalized to the area of each ROI (GFP intensity/glomeruli area) to calculate the EG invasion in each glomerulus. Then, the normalized GFP intensity of each glomerulus of an antennal lobe was summed and normalized for the

number of glomeruli detected in the antennal lobe. For each experiment, the EG antennal lobe invasion of each fly was normalized to the mean of the control. Representative images show the SUM projections of the 3 Z-planes.

Immunohistochemistry and confocal imaging – TH staining

Immunohistochemistry was performed on adult fly brains of 22±2-day-old, with at least two independent experiments. The brains were dissected in ice-cold PBS and fixed for 20 min in freshly prepared 3.7% paraformaldehyde (in 1x PBS, 0.2% Triton X-100 [PBX]) at room temperature (RT), followed by three 15-min washes in PBX at RT on a shaker. Then, the brains were incubated for 1 h in blocking solution (PBX, 10% normal goat serum [NGS]) at RT. Following blocking, the brains were incubated with primary antibodies (rabbit anti-TH [Sigma], 1:200, mouse anti-DLG [DSHB], 1:100) in blocking solution at 4°C for 1.5 to 2 days, followed by three 15-min washes in PBX at RT. Secondary antibodies (goat anti-rabbit Alexa488, goat anti-mouse Alexa555, both at 1:500 [Thermo Fisher Scientific]) in PBX with 10% NGS were applied overnight at 4°C. Afterwards, the brains were washed three times for 15 min in PBT at RT on a shaker and mounted with the anterior facing up in RapiClear 1.47 (SUNJin Lab). Imaging was performed using a Nikon A1R confocal microscope with a 20x (NA0.95) water immersion lens; Z-stacks of the entire brain were acquired. The acquisition was carried out using a Galvano scanner, with a zoom factor of 1, scan speed of 0.5, and line averaging set to 2. All images were captured with a pinhole of 2.3 Airy units and a resolution of 1024 × 1024. Z-stacks (with 3 µm step intervals) were obtained for data acquisition, and the same imaging settings were applied across all genotypes and sessions. Image analysis was performed using Fiji (Schindelin et al., 2009). To quantify dopaminergic neuron innervation of the mushroom body (MB), anti-DLG was used to identify the five Z-planes containing the synaptic region of the MB lobes. The ROI for the MB was defined in the sum projection of the five z-planes. To exclude background signal comparable to control, the area of anti-TH fluorescence was thresholded (using the default threshold for all z-planes) within the selected z-stacks. Quantification of the thresholded area within the ROI was performed in each z-plane, then summed and normalized to the MB ROI area for each brain individually (TH+ area/MB area). For each experiment, the individual TH+ area/MB area values were normalized to the mean of the control. Representative images show the maximum projection of five z-planes and the thresholded middle z-plane.

Electroretinograms (ERG)

ERGs were recorded from flies 5±1-day-old as previously described (Heisenberg, 1971; Slabbaert et al., 2016). Flies were immobilized on glass microscope slides using double-sided tape. For recordings, glass electrodes (borosilicate, 1.5 mm outer diameter) filled with 3 M NaCl were placed in the thorax as a reference and on the fly eye for recordings. Each fly was exposed to 5 cycles of 3 s of darkness, followed by a 1-s of light stimuli with LED illumination. Response to the stimuli was recorded using Axoscope 10.7 and analyzed using Clampfit 10.7 software (Molecular Devices). ERG traces were analyzed with Igor Pro 6.37 (Wave Metrics) using a custom-made macro.

Single-cell dissociation for cell-type specific transcriptomics

To test that EG could be isolated from the rest of the brain, we used two cohorts *GMR56F03> UAS-His2Av::eGFP.VK27* and *nSyb-Gal4> UAS-His2Av::eGFP.VK27*. To identify differentially expressed genes in EG, two cohorts were used: the control w^{1118} expressing GMR56F03> UAS-His2Av::eGFP.VK27 and $Pink1^{KO\text{-}WS}$ expressing *GMR56F03> UAS-His2Av::eGFP.VK27*. For each genotype, ten brains of flies 5±1-day-old were collected, with most of the laminae removed, from each experimental repeat. The dissections were performed in ice-cold PBS that contained 5 µM Actinomycin D (Sigma) to inhibit changes in gene expression during tissue processing(Y. E. Wu et al., 2017). To prevent any bias caused by different experimental batches, all the genotypes were processed in parallel. To minimize variability across batches, the same reagents and procedures

were used throughout the experiment. Dissections were completed within one hour. The dissection order and the assignment of genotypes to dissectors were alternated to reduce any experimenter-related variation.

For the dissociation of brain tissue, a mix of Dispase I (0.6 mg/ml) (Sigma), Collagenase I (30 mg/ml) (Thermo Fisher), Trypsin (0.5x) (Thermo Fisher), and 5 µM Actinomycin D was used. The brains were incubated for 20 min at 25°C with 1000 rpm shaking, performing four triturations at 5-min intervals. After dissociation, the cell suspension was washed with PBS containing 5 µM Actinomycin D and then filtered through a 10 µm strainer (Pluriselect), using 300 µl of PBS EDTA (Sigma) 1µM. DAPI (Sigma) (1:300.000) was added after filtration.

Fluorescence Activated Cell Sorting (FACS) for cell-type specific transcriptomics

Immediately after the dissociation, cells were sorted using a FACSAria Fusion (BD Biosciences) flow cytometer equipped with 4 lasers (405nm, 488nm, 561nm and 640nm) and a 100 µm nozzle at 20 psi. Live (DAPI-negative), GFP-positive cells were sorted into 96-well PCR plates at 300 cells per well (3 wells per genotype) using a 4-way purity mask with the FACSDiva software v9.0.1 (BD Biosciences).

Bulk transcriptomics of EG cells

Library preparations and sequencing for the Bulk RNA seq of the EG cells were performed using a modified Smart-seq2 protocol based on a previously published protocol (Picelli et al., 2013). Briefly, 3 µl of cell lysis buffer (0.1% Triton X-100, Sigma Aldrich; 1U/ul of RNase Inhibitor, RNase OUT, Thermo Fisher; 2.5 µM Oligo dT(25), IDT; and 2.5 mM dNTP, Promega) was aliquoted in triplicate to 96-well plates (4titude, Cat. No. 4TI-0960/C). Roughly 300 cells were sorted into the wells with lysis buffer and the plate was spun down at 2000xg for 1 min prior to storage at -80 °C. For the first strand synthesis, the Smart-Seq 2 plates were thawed to RT for a minute and subsequently spun down at 2000 xg for a minute. The RNA denaturation is carried out at 72°C for 10 min and then flash cooled on ice for 5 min. First strand synthesis mix (1X SuperScript II first strand synthesis buffer, Thermo Fisher; 5 mM DTT, Thermo Fisher; 100 U SuperScript II reverse transcriptase enzyme, Thermo Fisher; 10 U RNAse OUT, Thermo Fisher; 1M Betaine, Sigma Aldrich; 6 mM MgCl2, Thermo Fisher; and 1 uM TSO, IDT Technologies) is added to the cell lysis mix to a total volume of 10 µl. The First strand synthesis reaction was carried out with following program: 42°C for 90 min; 10 cycles of {50°C for 2 min; 42°C for 2 min}; 72°C for 15 min; 4°C indefinite hold. PCR amplification of the first strand product was performed by adding 15 µl of the PCR mix to the first strand product (1X KAPA HiFi HotStart Ready Mix, Roche; and 0.1 µM of IS PCR primer, IDT Technologies). 22 cycles of the following PCR program were used to amplify the first strand product: 98°C for 3 min; 22 cycles of {98°C for 20 sec; 67°C for 15 sec; 72°C for 6 min}; 72°C for 5 min; 4C indefinite hold. 20 µl of Ampure XP was added to each well and mixed. Standard Ampure XP purification was carried out as per manufacturer's recommendation, and the cDNA library was eluted in 17.5 µl of Elution buffer. 17 µl of the eluted library was,transferred to a fresh 96-well plate (4titude, Cat. No. 4TI-0960/C). 5 µl of Tn5 tagmentation mix (1X Tagment DNA buffer, Illumina; ATM mix, Illumina, and cDNA library 1 ng) was prepared for cDNA fragmentation. Tn5 tagmentation was performed with the following program: 55°C for 10 min; 4°C indefinite hold. Tagmentation reaction was stopped by quenching the reaction with 1.25 µl of NT buffer for 5 min (Illumina). 1.25 µl of the i5 and i7 Illumina indexes were added to the plates. Finally 3.75 µl of NPM master mix was added to the plate and mixed well and put for the index PCR amplification: 72°C for 3 min; 95°C for 30 sec; 12 cycles of {95°C for 10 sec; 55°C for 30 sec; 72°C for 30 sec}; 72°C for 5 min, and 4°C indefinite hold.

The indexed PCR products were pooled in a single tube, and 0.8X Ampure XP purification (Beckman Coulter) was carried out as per the manufacturer's recommendation, and finally, the sequencing library was eluted in 35.5 µl of Elution buffer (Qiagen).

SMART seq 2 libraries were sequenced on the NextSeq 500 (Illumina) sequencing platform. Sequencing was done as per the protocol recommendations: paired-end read of 76 bps (read 1), 76 bps (read 2), 8 bps (index 1) and 8 bps (index 2). For a targeted sequencing depth of ~30 million reads per sample.

Analysis of RNAseq data - Neuron vs EG

Raw reads from neuron- vs. glia-specific FACsorting experiments were processed with the nf-core/rnaseq pipeline (Patel et al., 2020) with default parameters and the BDGP6 reference genome. The STAR-aligned and salmon-quantified expression matrix was then subset to genes known to be enriched in neurons or glia and displayed as a per gene scaled heatmap.

Analysis of RNAseq data - EG-specific differentially expressed genes

After FACsorting of $Pink^{KO\text{-}ws}$ vs. control ensheathing glia, library preparation and sequencing resulting FASTQ files were cleaned with fastp (Chen et al., 2018) with default settings. Aligning and counting were carried out with STAR (Dobin et al., 2013) and the 4th 2020 FlyBase *Drosophila melanogaster* release (r6.35) with the –quantMode flag set as GeneCounts. For differential gene expression testing we used DESeq2 (Love et al., 2014), where we fit a negative binomial model and carried out the Wald-test. We removed the experimental batch as a covariate according to the design formula ~date+genotype. All genes below a Benjamini-Hochberg corrected p-value of 0.05 were considered deregulated.

ScRNAseq data loading, filtering, clustering, and differential expression analysis

Raw counts data from (Pech et al., 2025), alongside cell annotations provided by the authors, was loaded into Scanpy (v1.9.1) (Wolf et al., 2018) and subset to only include cells in the young control (<= 6-day-old) or $Pink1^{KO\text{-}WS}$ samples. After subsetting the data, filtering was performed to remove any cell with less than 250 genes expressed or a percentage of counts coming from mitochondrial genes greater than 15%, the data was then normalized to a total of 10.000 counts and log transformed. Highly variable genes were detected, total_counts and percent of mitochondrial reads were regressed out, and finally the data was scaled to unit variance with a zero mean, clipped to a max of 10.

After data pre-processing, a PCA was performed, Harmony (Korsunsky et al., 2019) was used to correct batches using “sample_id” as a batch key, and 122 components were used for dimensionality reduction and clustering analyses. Leiden clustering was performed with a resolution of 8.0 and using the annotations from (Pech et al., 2025), all cells within each cluster were labeled by taking the most common, original annotation per cluster.

Per cluster, a differential analysis was performed. First, pseudobulk counts were generated by summing the counts per cell from all cells per sample. These counts were then used in DESeq2 (v1.44.0) (Love et al., 2014) comparing Control vs $Pink1^{KO\text{-}WS}$ samples. The total number of genes significantly up- or downregulated per cluster (padj <= 0.05 and an abs (log2foldchange) >= 1.5) was counted and plotted.

Statistical analysis

GraphPad Prism was used for visualization and to determine statistical significance. Datasets were tested for normal distribution using the D’Agostino-Person Omnibus and the Shapiro-Wilk normality test. For a normally distributed dataset ordinary one-way ANOVA was used, followed to correct for multiple comparisons by a post hoc Tukey’s test when comparing all the datasets with each other or Dunnett’s test when comparing all the datasets to a general control. For non-normally distributed datasets Kruskal-Wallis test is used, followed by a post hoc Dunn’s test to correct for multiple comparisons. Significance levels are defined as * is $p<0.05$, ** is $p<0.01$, *** is $p<0.001$, and ns, not significant. Effect size is calculated with eta-squared when one-way ANOVA is

used, indicated in the figure legend as η. 'N' in the legends is used to indicate how many animals were analyzed. Data are plotted as mean ± SD. Specifics on the statistical test used for each analysis are reported in the figure legends.

Key resources table

Reagent type (species) or resource	Designation	Source or reference	Identifier	Additional information
Antibody	Rabbit polyclonal anti-GFP	Thermo Fisher Scientific	Cat#A-11122; RRID: AB_221569	
Antibody	Mouse monoclonal anti-Brp	DSHB	Cat#nc82; RRID: AB_2314866	
Antibody	Mouse monoclonal anti-DLG	DSHB	Cat#4F3; RRID: AB 528203	
Antibody	Rabbit polyclonal anti-TH	Sigma Aldrich	Cat#AB 152	
Antibody	Alex Flour 488 goat anti-rabbit	Invitrogen	Cat#A11034	
Antibody	Alexa Fluor 555 goat anti-mouse IgG2a	Invitrogen	Cat#A21137	
Commercial assay, kit	Agencourt AMPure XP	Beckman Coulter	Cat#A63880	
Commercial assay, kit	KAPA HiFi HotStart ReadyMix	Roche	Cat# 07958927001	

Commercial assay, kit	Nextera XT DNA Library Preparation Kit	Illumina	Cat#FC-131-1096	
Peptide, recombinant protein	Dispase I	Sigma Aldrich	Cat#D4818	
Peptide, recombinant protein	Collagenese I	Thermo Fisher Scientific	Cat#17100017	
Peptide, recombinant protein	SuperScript™ II Reverse Transcriptase	Thermo Fisher Scientific	Cat#18064022	
Chemical compound, drug	Trypsin-EDTA (0,5%)	Thermo Fisher Scientific	Cat#15400054	
Chemical compound, drug	Triton X-100 Solution	Sigma Aldrich	Cat#93443-100Ml	
Chemical compound, drug	Paraformaldehyde	Sigma Aldrich	Cat#252549	
Chemical compound, drug	Actinomycin D	Sigma Aldrich	Cat#A1410	
Chemical compound, drug	EDTA	Sigma Aldrich	Cat#E6511	
Chemical compound, drug	DAPI	Sigma Aldrich	Cat#D9542	
Chemical compound, drug	$MgCl_2$ (1M)	Thermo Fisher Scientific	Cat#AM9530G	
Chemical compound, drug	RNaseOUT	Thermo Fisher Scientific	Cat#10777019	
Chemical compound, drug	Betaine	Sigma Aldrich	Cat#B0300	
Chemical compound, drug	DTT (100mM Solution)	Thermo Fisher Scientific	Cat#707265ML	
Chemical compound, drug	Buffer EB	Qiagen	Cat#19086	
Chemical compound, drug	RapiClear 1.47	Sunjin Lab	Cat#RC147001	
Sequence-based reagent	dNTP Mix	Promega	Cat#U1511	
Sequnce-based reagent	Primers, gRNAs, oligos, gBlocks	Integrated DNA technologies (IDT)		
Strain, strain backgrou	*w[1118]* (w^{1118})	(Kaempf et al., 2026)	NA	

nd (*D. melanogaster*)				
Strain, strain background (*D. melanogaster*)	*w[1118] M{w+} (w^{1118} w+)*	(Kaempf et al., 2026)	NA	
Gene (*D. melanogaster*)	*w[1118] TI{w[+]=white-STAR}Pink1[KO-WS]/FM7a ($Pink1^{KO-WS}$)*	(Kaempf et al., 2026)	NA	
Genetic reagent (*D. melanogaster*)	*Yw; ; UAS-His2Av::eGFP.VK27/TM3Sb (UAS-HisTag-eGFP)*	This study	NA	
Genetic reagent (*D. melanogaster*)	*;;MZ0709-Gal4*	(Ito et al., 1995)	NA	
Genetic reagent (*D. melanogaster*)	*y[1] w[*]; P{w[+mC]=UAS-mCD8::GFP.L}LL5, P{UAS-mCD8::GFP.L}2 (UAS-mCD8-GFP)*	(Lee & Luo, 1999)	BDSC_5137	
Genetic reagent (*D. melanogaster*)	*w[*]; P{y[+t7.7] w[+mC]=GMR56F03-GAL4}attP24/CyO (Gmr56-gal4)*	(Jenett et al., 2012)	BDSC_77469	
Genetic reagent (*D. melanogaster*)	*y[1] v[1]; P{y[+t7.7] v[+t1.8]=TRiP.JF01672}attP2 ($Pink1^{RNAi}$)*	(Perkins et al., 2015)	BDSC_31170	
Genetic reagent (*D. melanogaster*)	*w[*]; P{w[+mC]=UAS-Pink1.C}A (UAS-Pink1)*	Bloomington Drosophila Stock Center	BDSC_51648	
Genetic reagent (*D. melanogaster*)	*w[1118]; P{y[+t7.7] w[+mC]=GMR57C10-GAL4}attP2 (nSyb-gal4)*	(Jenett et al., 2012)	BDSC_39171	
Genetic reagent (*D. melanogaster*)	*y[1] sc[*] v[1] sev[21]; P{y[+t7.7] v[+t1.8]=TRiP.HMS02460}attP40 ($Vps13^{RNAi}$)*	(Perkins et al., 2015)	BDSC_38270	
Genetic reagent (*D. melanogaster*)	*y[1] sc[*] v[1] sev[21]; P{y[+t7.7] v[+t1.8]=TRiP.HMS01858}attP40 ($Vps35^{RNAi}$)*	(Perkins et al., 2015)	BDSC 38944	
Genetic reagent (*D. melanogaster*)	*y[1] sc[*] v[1] sev[21]; P{y[+t7.7] v[+t1.8]=TRiP.HMS05488}attP40 ($CG17660^{RNAi}$)*	(Perkins et al., 2015)	BDSC_67022	

Genetic reagent (*D. melanogaster*)	*y[1] v[1]; P{y[+t7.7] v[+t1.8]=TRiP.JF03249}attP2 (Proc^{RNAi})*	(Perkins et al., 2015)	BDSC_29570	
Genetic reagent (*D. melanogaster*)	*y[1] sc[*] v[1] sev[21]; P{y[+t7.7] v[+t1.8]=TRiP.HMC05229}attP40 (fiz^{RNAi})*	(Perkins et al., 2015)	BDSC_62222	
Genetic reagent (*D. melanogaster*)	*y[1] v[1]; P{y[+t7.7] v[+t1.8]=TRiP.JF01165}attP2 (CG15011^{RNAi})*	(Perkins et al., 2015)	BDSC_31589	
Genetic reagent (*D. melanogaster*)	*y[1] sc[*] v[1] sev[21]; P{y[+t7.7] v[+t1.8]=TRiP.HMC04857}attP40 (CG17612^{RNAi})*	(Perkins et al., 2015)	BDSC_57540	
Genetic reagent (*D. melanogaster*)	*y[1] sc[*] v[1] sev[21]; P{y[+t7.7] v[+t1.8]=TRiP.HMC05717}attP40 (Prpk^{RNAi})*	(Perkins et al., 2015)	BDSC 64844	
Genetic reagent (*D. melanogaster*)	*y[1] v[1]; P{y[+t7.7] v[+t1.8]=TRiP.HMJ22434}attP40 (Lnpk^{RNAi})*	(Perkins et al., 2015)	BDSC_64036	
Genetic reagent (*D. melanogaster*)	*y[1] sc[*] v[1] sev[21]; P{y[+t7.7] v[+t1.8]=TRiP.HMS01827}attP2 (PIG-B^{RNAi})*	(Perkins et al., 2015)	BDSC_38359	
Genetic reagent (*D. melanogaster*)	*y[1] sc[*] v[1] sev[21]; P{y[+t7.7] v[+t1.8]=TRiP.HMS01840}attP2/TM3, Sb[1] (spag^{RNAi})*	(Perkins et al., 2015)	BDSC_38371	
Genetic reagent (*D. melanogaster*)	*y[1] sc[*] v[1] sev[21]; P{y[+t7.7] v[+t1.8]=TRiP.HMS00070}attP2 (Rel^{RNAi})*	(Perkins et al., 2015)	BDSC_33661	
Genetic reagent (*D. melanogaster*)	*y[1] v[1]; P{y[+t7.7] v[+t1.8]=TRiP.JF03249}attP2 (Proc^{RNAi})*	Bloomington Drosophila Stock Center	BDSC 29570	
Genetic reagent (*D. melanogaster*)	*y[1] sc[*] v[1] sev[21]; P{y[+t7.7] v[+t1.8]=TRiP.HMC04640}attP40 (Atac1^{RNAi})*	(Perkins et al., 2015)	BDSC_57250	
Genetic reagent (*D. melanogaster*)	*y[1] sc[*] v[1] sev[21]; P{y[+t7.7] v[+t1.8]=TRiP.GLV21056}attP2 (l(3)07882^{RNAi})*	(Perkins et al., 2015)	BDSC_35691	
Genetic reagent (*D.*	*y[1] sc[*] v[1] sev[21]; P{y[+t7.7] v[+t1.8]=TRiP.HMS00529}*	(Perkins et al., 2015)	BDSC_32839	

melanogaster)	*attP2 (Pld^{RNAi})*			
Genetic reagent (*D. melanogaster)*	*y[1] sc[*] v[1] sev[21]; P{y[+t7.7] v[+t1.8]=TRiP.HMS02243} attP2 (Rpp25^{RNAi})*	(Perkins et al., 2015)	BDSC_41679	
Genetic reagent (*D. melanogaster)*	*y[1] v[1]; P{y[+t7.7] v[+t1.8]=TRiP.HMC03184} attP40 (GMF^{RNAi})*	(Perkins et al., 2015)	BDSC_51452	
Genetic reagent (*D. melanogaster)*	*y[1] sc[*] v[1] sev[21]; P{y[+t7.7] v[+t1.8]=TRiP.HMS01358} attP2/TM3, Sb[1] (Atg7^{RNAi})*	(Perkins et al., 2015)	BDSC_34369	
Genetic reagent (*D. melanogaster)*	*y[1] v[1]; P{y[+t7.7] v[+t1.8]=TRiP.HMJ03126}attP40 (Ada2a^{RNAi})*	(Perkins et al., 2015)	BDSC_50905	
Genetic reagent (*D. melanogaster)*	*y[1] sc[*] v[1] sev[21]; P{y[+t7.7] v[+t1.8]=TRiP.HMC06224} attP2 (CG12773^{RNAi})*	(Perkins et al., 2015)	BDSC_65949	
Genetic reagent (*D. melanogaster)*	*y[1] sc[*] v[1] sev[21]; P{y[+t7.7] v[+t1.8]=TRiP.HMS00328} attP2 (CG7627^{RNAi})*	(Perkins et al., 2015)	BDSC_32337	
Genetic reagent (*D. melanogaster)*	*y[1] v[1]; P{y[+t7.7] v[+t1.8]=TRiP.HMS00870} attP2 (Dark^{RNAi})*	(Perkins et al., 2015)	BDSC_33924	
Genetic reagent (*D. melanogaster)*	*y[1] v[1]; P{y[+t7.7] v[+t1.8]=TRiP.JF03275}attP2 (CG3703^{RNAi})*	(Perkins et al., 2015)	BDSC_29596	
Genetic reagent (*D. melanogaster)*	*y[1] sc[*] v[1] sev[21]; P{y[+t7.7] v[+t1.8]=TRiP.HMS01175} attP2/TM3, Sb[1] (NiPp1^{RNAi})*	(Perkins et al., 2015)	BDSC_34696	
Genetic reagent (*D. melanogaster)*	*y[1] v[1]; P{y[+t7.7] v[+t1.8]=TRiP.HMJ22813}attP40 (CG31370^{RNAi})*	(Perkins et al., 2015)	BDSC_60456	
Genetic reagent (*D. melanogaster)*	*y[1] v[1]; P{y[+t7.7] v[+t1.8]=TRiP.HMJ23526}attP40 (Irbp^{RNAi})*	(Perkins et al., 2015)	BDSC_61942	
Genetic reagent (*D. melanogaster)*	*y[1] v[1]; P{y[+t7.7] v[+t1.8]=TRiP.JF02313}attP2 (CG32532^{RNAi})*	Click or tap here to enter text.	BDSC_26750	
Genetic	*y[1] v[1]; P{y[+t7.7]*	(Perkins	BDSC 62936	

reagent (*D. melanogaster*)	*v[+t1.8]=TRiP.HMJ30013}attP40/CyO (Rhau^{RNAi})*	et al., 2015)		
Genetic reagent (*D. melanogaster*)	*y[1] v[1]; P{y[+t7.7] v[+t1.8]=TRiP.HM05047}attP2 (hfw^{RNAi})*	(Perkins et al., 2015)	BDSC_28561	
Genetic reagent (*D. melanogaster*)	*y[1] v[1]; P{y[+t7.7] v[+t1.8]=TRiP.JF02192}attP2 (achi^{RNAi})*	(Perkins et al., 2015)	BDSC_31903	
Genetic reagent (*D. melanogaster*)	*y[1] v[1]; P{y[+t7.7] v[+t1.8]=TRiP.HMJ23972}attP40/CyO (TTLL6A^{RNAi})*	(Perkins et al., 2015)	BDSC_62488	
Genetic reagent (*D. melanogaster*)	*y[1] sc[*] v[1] sev[21]; P{y[+t7.7] v[+t1.8]=TRiP.HMC03076}attP2 (Nos^{RNAi})*	(Perkins et al., 2015)	BDSC_50675	
Genetic reagent (*D. melanogaster*)	*w[1118]; P{w[+mC]=UAS-Nos.L}2 (UAS-Nos)*	Bloomington Drosophila Stock Center	BDSC_56823	
Plasmids	pUASTattB	(Bischof, 2007)	https://www.flyc31.org	
Software, algorithm	Fiji	(Schindelin et al., 2009)	RRID:SCR_002285	https://imagej.net/Fiji
Software, algorithm	GraphPad Prism	GraphPad software, CA, USA	RRID:SCR_002798	https://www.graphpad.com/scientific-software/prism/
Software, algorithm	Python (v 3.7.3)	Python	RRID:SCR_008394	http://www.python.org/
Software, algorithm	scanpy	(Wolf et al., 2018)	RRID:SCR_018139	https://github.com/theislab/scanpy
Software, algorithm	DESeq2	(Love et al., 2014)	RRID:SCR_015687	https://bioconductor.org/packages/release/bioc/html/DESeq2.html
Software, algorithm	Clampfit	Molecular Devices		https://www.moleculardevices.com
Software, algorithm	Axoscope	Molecular Devices		https://www.moleculardevices.com
Software, algorithm	Igor Pro	WaveMetrics	RRID: CR_000325	https://www.wavemetrics.com/products/igorpro/igorpro.htm
Software, algorithm	FACSDiva software v9.0.1	BD Biosciences	RRID:SCR_001456	https://www.bdbiosciences.com/en-be/products/software/instrument-software/bd-facsdiva-software
Software, algorithm	nf-core/rnaseq	(Patel et al., 2020)		https://nf-co.re/rnaseq/3.14.0/
Software, algorithm	fastp	(Chen et al., 2018)		https://github.com/OpenGene/fastp
Software, algorithm	R Studio	RStudio, PBC / Posit		
Software, algorithm	BioRender	BioRender		https://BioRender.com
Software, algorithm	STAR	(Dobin et al., 2013)	RRID:SCR_004463	https://github.com/alexdobin/STAR
Software, algorithm	Harmony	(Korsunsky et al., 2019)		https://github.com/immunogenomics/harmony

Supplementary figures

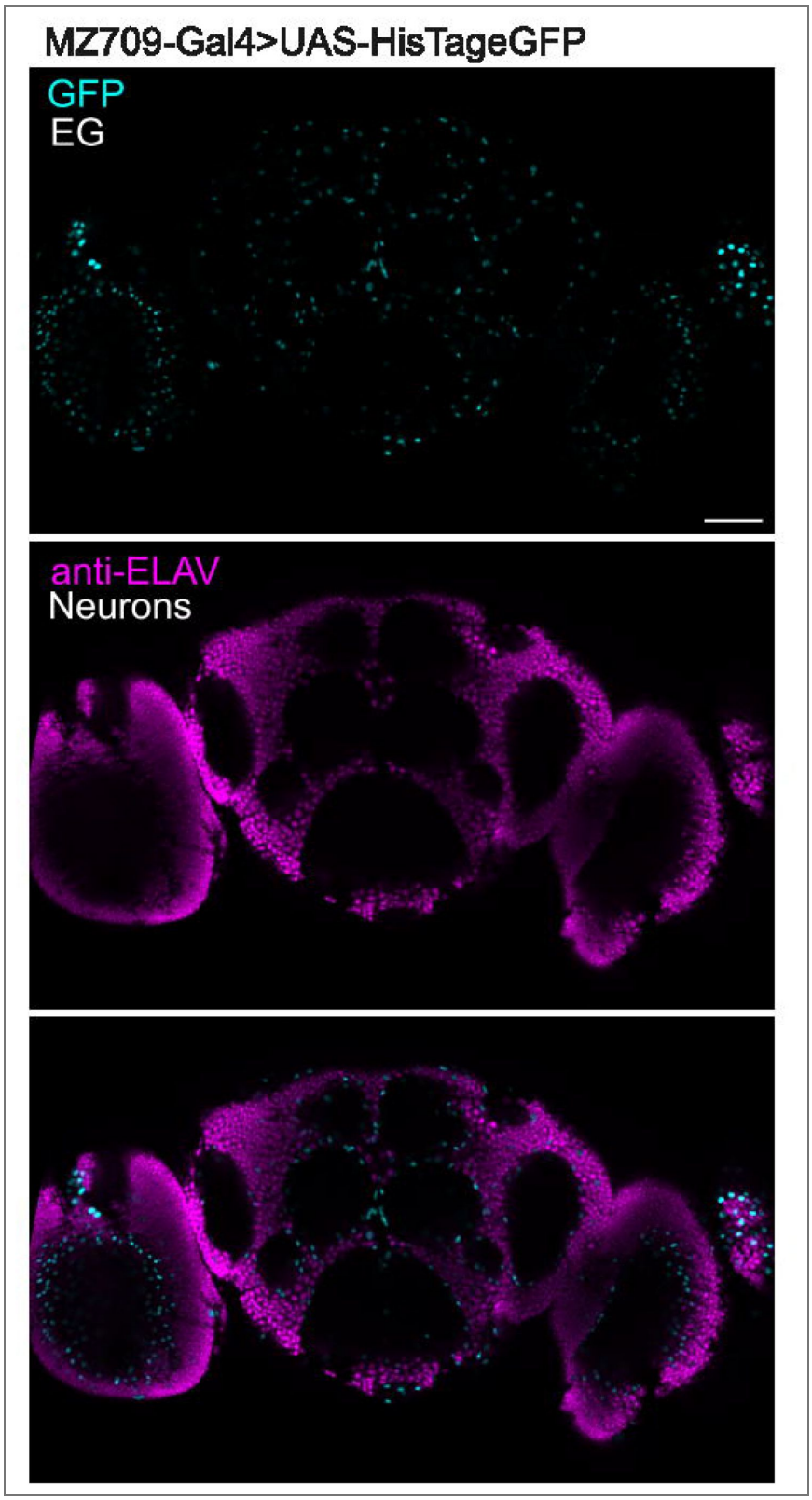

Supplementary Figure 1. Representative confocal image of a (5 ± 1-day-old) MZ709-Gal4/+;; UAS-HisTageGFP/+ brain stained with anti-GFP (Cyan) and anti-ELAV (Magenta). Scale bar: 50μm; N= 3, 1 replicate.

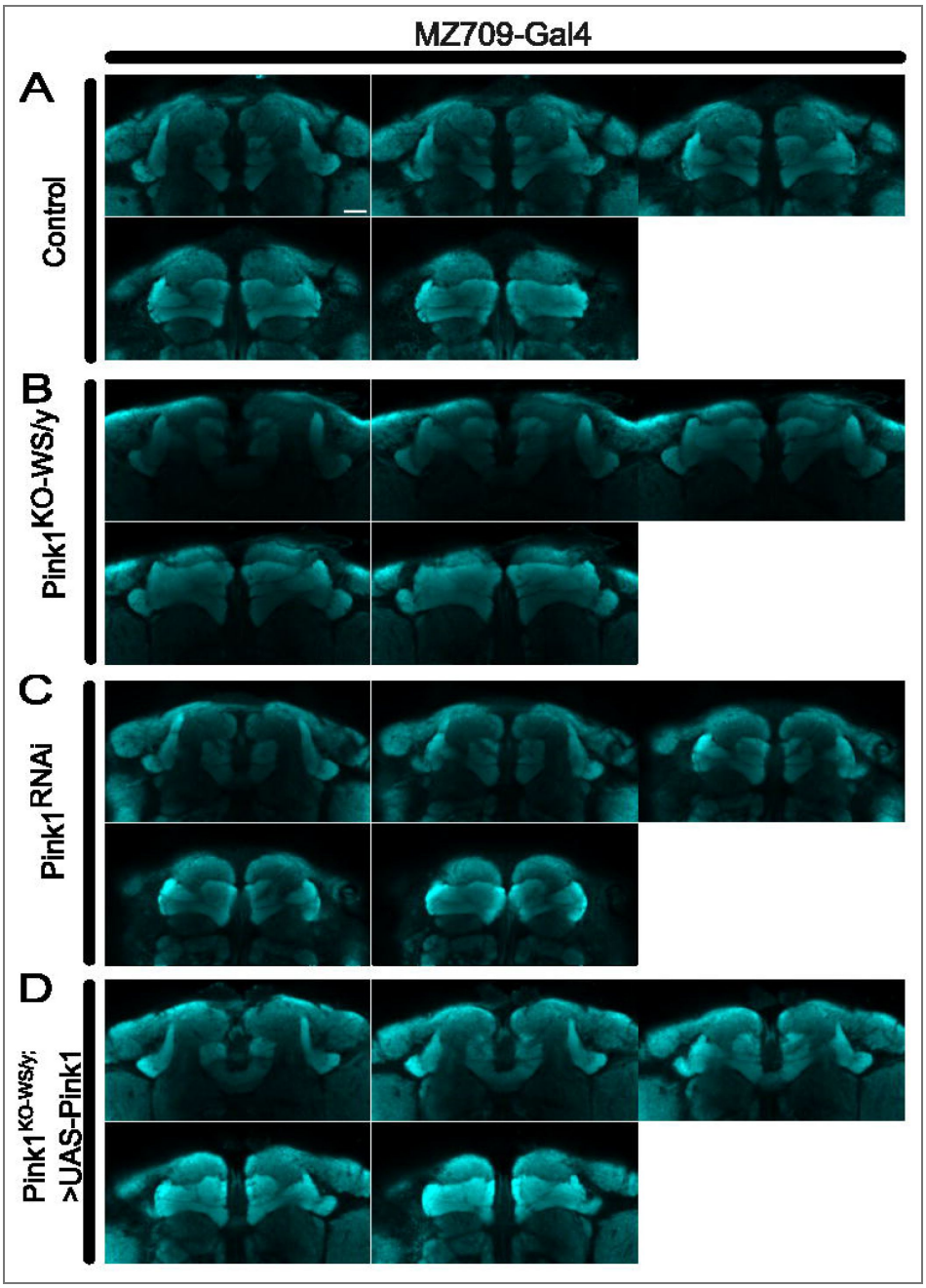

Supplementary Figure 2. Examples of confocal Z-stacks of anti-DLG labeled fly brains (22 ± 2-day-old) of the indicated genotypes.

Such images were used to delineate ROIs to quantify DAN innervation onto the MBs. (A) control (w1118/y;; MZ709-Gal4/+); (B) Pink1KO-WS/Y;; MZ709-Gal4/+; (C) flies where *Pink1* is downregulated in EG (w1118/y;; MZ709-Gal4/ Pink1RNAi); (D) Pink1KO-WS flies with expression of wild type *Pink1* in EG (Pink1KO-WS/Y;; MZ709-Gal4/UAS-Pink1).

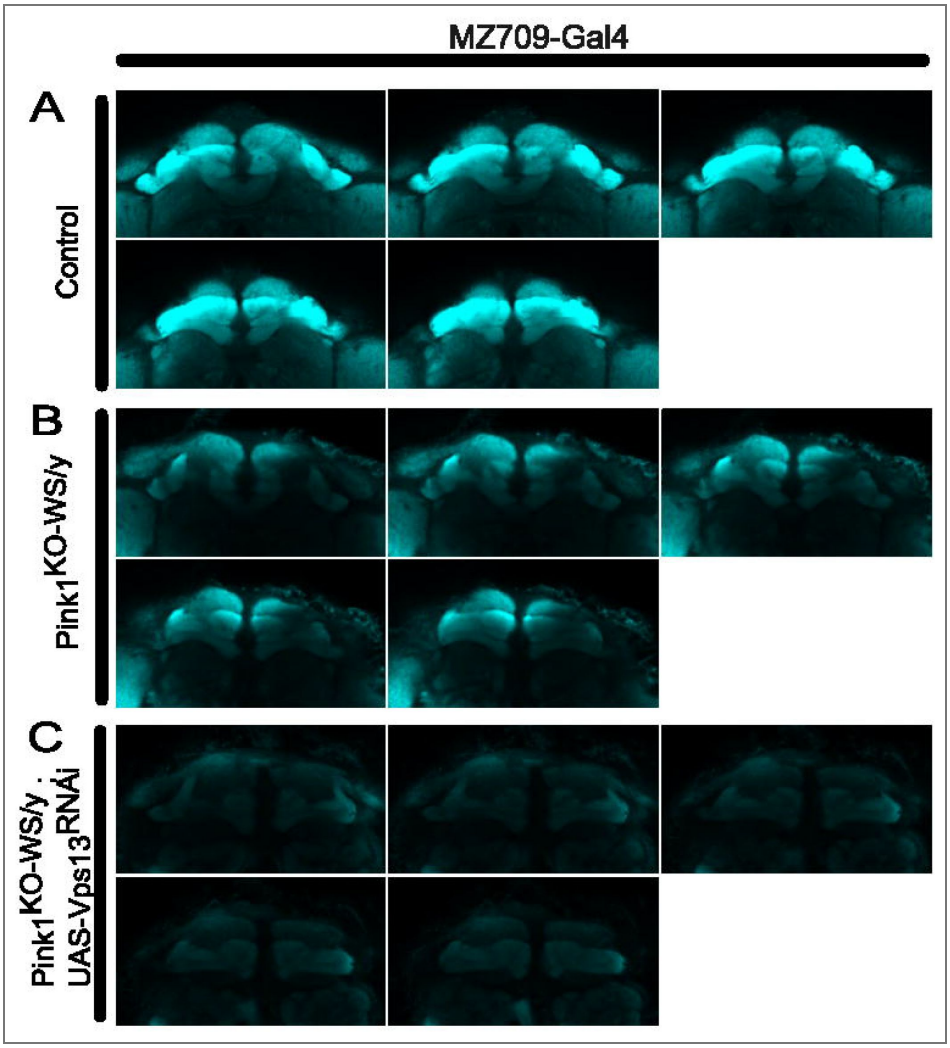

Supplementary Figure 3. Examples of confocal Z-stacks of anti-DLG labeled fly brains (22 ± 2-day-old) of the indicated genotypes.

Such images were used to delineate ROIs to quantify DAN innervation onto the MBs. (A) control (w1118/y;; MZ709-Gal4/+); (B) Pink1KO-WS/Y;; MZ709-Gal4/+; (C) Pink1KO-WS flies with *Vps13* downregulation in EG (Pink1KO-WS/Y;; *Vps13*RNAi/MZ709-Gal4).

Data availability

RNA sequence data were deposited in GEO (accession number GSE322929). All data generated or analyzed during this study are included in the manuscript and supporting files; source data file has been provided for all figures.

Acknowledgements

We thank the Vlaams Supercomputer Centrum, the VIB Nucleomic and Bioimaging Cores, and the Bloomington *Drosophila* Stock Center (NIH P40OD018537). We are grateful to the members of the Verstreken lab for valuable discussions. Research support was provided by Leuven University Fund and Opening the Future, ERC, the Chan Zuckerberg Initiative, a Methusalem grant from the Flemish government, KU Leuven BOF, Fund Jacqueline Cigrang administered by the KBS, the KBS, fund Generet and FWO Vlaanderen to PV an EMBO long-term fellowship to RP, a DFG fellowship to UP and an FWO PhD mandate to AK. Cartoons/models/illustrations were created in *https://BioRender.com*. P.V. is an alumnus of the FENS-Kavli Network of Excellence.

Additional information

Funding

Leuven University Fund and Opening the Future, ERC, the Chan Zuckerberg Initiative, a Methusalem grant from the Flemish government, KU Leuven BOF, Fund Jacqueline Cigrang administered by the KBS, the KBS, fund Generet and FWO Vlaanderen to PV

EMBO long-term fellowship to RP

DFG fellowship to UP

FWO PhD mandate to AK

Author contributions

Conceptualization, L.G., R.P., P.V.;

Methodology, L.G., U.P., N.S., J.L., K.D., R.P., P.V., S.K., A.K.;

Software, L.G., K.D., R.P.;

Validation, L.G., K.D., R.P.;

Formal analysis, L.G., K.D., R.P.;

Investigation, L.G., U.P., N.S., J.L., K.D., R.P., S.K., A.K.;

Writing -Original Draft, L.G., R.P., P.V.;

Writing – review and editing, all co-authors read and edited the manuscript.

Visualization, L.G., K.D., R.P., S.K.;

Supervision, R.P., P.V.;

Project administration, L.G.;

Funding acquisition, R.P., P.V.;

Inclusion and diversity

We support inclusive, diverse, and equitable conduct of research.

Funding

Funder	Grant reference number	Author
KU Leuven (Katholieke Universiteit Leuven)		Patrik Verstreken
EC | European Research Council (ERC)		Patrik Verstreken

Chan Zuckerberg Initiative (CZI)	Patrik Verstreken
Vlaamse Overheid (Government of Flanders)	Patrik Verstreken
Koning Boudewijnstichting (kbs-frb)	Patrik Verstreken
Fonds Wetenschappelijk Onderzoek (FWO)	Patrik Verstreken
European Molecular Biology Organization (EMBO)	Roman Praschberger
Deutsche Forschungsgemeinschaft (DFG)	Ulrike Pech
Fonds Wetenschappelijk Onderzoek (FWO)	Ayse Kilic

Author ORCID iDs

Patrik Verstreken: https://orcid.org/0000-0002-5073-5393

Additional files

Appendix 1.

Supplementary Table 1.

Source Data 1.

References

Agarwal D, Sandor C, Volpato V, Caffrey TM, Monzón-Sandoval J, Bowden R, Alegre-Abarrategui J, Wade-Martins R, Webber C (2020) A single-cell atlas of the human substantia nigra reveals cell-specific pathways associated with neurological disorders. *Nature Communications* **11**:1-11 https://doi.org/10.1038/s41467-020-17876-0 | PubMed

Barazzuol L, Giamogante F, Brini M, Calì T (2020) PINK1/Parkin Mediated Mitophagy, Ca2+ Signalling, and ER-Mitochondria Contacts in Parkinson's Disease. *International Journal of Molecular Sciences* **21** https://doi.org/10.3390/ijms21051772 | PubMed

Bischof J, Maeda RK, Hediger M, Karch F, Basler K (2007) An optimized transgenesis system for Drosophila using germ-line-specific ΦC31 integrases. *Proceedings of the National Academy of Sciences of the United States of America* **104**:3312-3317 https://doi.org/10.1073/pnas.0611511104 | PubMed

Brickner JH, Fuller RS (1997) SOI1 encodes a novel, conserved protein that promotes TGN-endosomal cycling of Kex2p and other membrane proteins by modulating the function of two TGN localization signals. *Journal of Cell Biology* **139**:23-36 https://doi.org/10.1083/jcb.139.1.23 | PubMed

Bryois J, Skene NG, Hansen TF, Kogelman LJA, Watson HJ, Liu Z, Adan R, Alfredsson L, Ando T, Andreassen O, *et al.* (2020) Genetic identification of cell types underlying brain complex traits yields insights into the etiology of Parkinson's disease. *Nature Genetics* **52**:482-493 https://doi.org/10.1038/s41588-020-0610-9 | PubMed

Chen S, Zhou Y, Chen Y, Gu J (2018) Fastp: An ultra-fast all-in-one FASTQ preprocessor. *Bioinformatics* **34**:i884-i890 https://doi.org/10.1093/bioinformatics/bty560 | PubMed

De Brito OM, Scorrano L (2008) Mitofusin 2 tethers endoplasmic reticulum to mitochondria. *Nature* **456**:605-610 https://doi.org/10.1038/nature07534 | PubMed

Delgado MG, Oliva C, López E, Ibacache A, Galaz A, Delgado R, Barros LF, Sierralta J (2018) Chaski, a novel Drosophila lactate/pyruvate transporter required in glia cells for survival under nutritional stress. *Scientific Reports* **8**:1-13 https://doi.org/10.1038/s41598-018-19595-5 | PubMed

Dobin A, Davis CA, Schlesinger F, Drenkow J, Zaleski C, Jha S, Batut P, Chaisson M, Gingeras TR (2013) STAR: Ultrafast universal RNA-seq aligner. *Bioinformatics* **29**:15-21 https://doi.org/10.1093/bioinformatics/bts635 | PubMed

Doherty J, Logan MA, Taşdemir ÖE, Freeman MR (2009a) Ensheathing Glia Function as Phagocytes in the Adult Drosophila Brain. *The Journal of Neuroscience* **29**:4768-4781 https://doi.org/10.1523/JNEUROSCI.5951-08.2009 | PubMed

Doherty J, Logan MA, Taşdemir ÖE, Freeman MR (2009b) Ensheathing Glia Function as Phagocytes in the Adult Drosophila Brain. *The Journal of Neuroscience* **29**:4768-4781 https://doi.org/10.1523/JNEUROSCI.5951-08.2009 | PubMed

Ettle B, Schlachetzki JCM, Winkler J (2016) Oligodendroglia and Myelin in Neurodegenerative Diseases: More Than Just Bystanders?. *Molecular Neurobiology* **53**:3046-3062 https://doi.org/10.1007/s12035-015-9205-3 | PubMed

Freeman MR, Doherty J (2006) Glial cell biology in Drosophila and vertebrates. *Trends in Neurosciences* **29**:82-90 https://doi.org/10.1016/j.tins.2005.12.002 | PubMed

Gaudet P, Livstone MS, Lewis SE, Thomas PD (2011) Phylogenetic-based propagation of functional annotations within the Gene Ontology consortium. *Briefings in Bioinformatics* **12**:449-462 https://doi.org/10.1093/bib/bbr042 | PubMed

Grossmann D, Malburg N, Glaß H, Weeren V, Sondermann V, Pfeiffer JF, Petters J, Lukas J, Seibler P, Klein C, *et al.* (2023) Mitochondria–Endoplasmic Reticulum Contact Sites Dynamics and Calcium Homeostasis Are Differentially Disrupted in PINK1-PD or PRKN-PD Neurons. *Movement Disorders* **38**:1822-1836 https://doi.org/10.1002/mds.29525 | PubMed

Ham SJ, Yoo H, Woo D, Lee DH, Park KS, Chung J (2023) PINK1 and Parkin regulate IP3R-mediated ER calcium release. *Nature Communications* **14** https://doi.org/10.1038/s41467-023-40929-z | PubMed

Hardie RC, Raghu P (2001) Visual transduction in Drosophila. *Nature* **413**:186-193 https://doi.org/10.1038/35093002 | PubMed

Heisenberg M (1971) Separation of receptor and lamina potentials in the electroretinogram of normal and mutant Drosophila. *Journal of Experimental Biology* **55**:85-100 https://doi.org/10.1242/jeb.55.1.85 | PubMed

Hirata T, Fujita M, Nakamura S, Gotoh K, Motooka D, Murakami Y, Maeda Y, Kinoshita T (2015) Post-Golgi anterograde transport requires GARP-dependent endosome-to-TGN retrograde transport. *Molecular Biology of the Cell* **26**:3071-3084 https://doi.org/10.1091/mbc.E14-11-1568 | PubMed

Ito K, Urban J, Technau GM (1995) Distribution, classification, and development of Drosophila glial cells in the late embryonic and early larval ventral nerve cord. *Roux's Archives of Developmental Biology* **204**:284-307 https://doi.org/10.1007/BF02179499 | PubMed

Jenett A, Rubin GM, Ngo T.-TB, Shepherd D, Murphy C, Dionne H, Pfeiffer BD, Cavallaro A, Hall D, Jeter J, *et al.* (2012) A GAL4-Driver Line Resource for Drosophila Neurobiology. *Cell Reports* **2**:991-1001 https://doi.org/10.1016/j.celrep.2012.09.011 | PubMed

Kaempf N, Valadas JS, Robberechts P, Schoovaerts N, Ortega A, Nachman E, Ghezzi L, Kilic A, Chabot D, Pech U, *et al.* (2026) Behavioral screening defines the molecular Parkinsonism subgroups in Drosophila. *Nature Communications* **17**:3761 https://doi.org/10.1038/s41467-026-70303-8 | PubMed

Kane LA, Lazarou M, Fogel AI, Li Y, Yamano K, Sarraf SA, Banerjee S, Youle RJ (2014) PINK1 phosphorylates ubiquitin to activate Parkin E3 ubiquitin ligase activity. *Journal of Cell Biology* **205**:143-153 https://doi.org/10.1083/jcb.201402104 | PubMed

Korsunsky I, Millard N, Fan J, Slowikowski K, Zhang F, Wei K, Baglaenko Y, Brenner M, Loh P. ru, Raychaudhuri S (2019) Fast, sensitive and accurate integration of single-cell data with Harmony. *Nature Methods* **16**:1289-1296 https://doi.org/10.1038/s41592-019-0619-0 | PubMed

Kremer MC, Jung C, Batelli S, Rubin GM, Gaul U (2017) The glia of the adult Drosophila nervous system. *Glia* **65**:606-638 https://doi.org/10.1002/glia.23115 | PubMed

Kumar N, Leonzino M, Hancock-Cerutti W, Horenkamp FA, Li P, Lees JA, Wheeler H, Reinisch KM, De Camilli P (2018) VPS13A and VPS13C are lipid transport proteins differentially localized at ER contact sites. *Journal of Cell Biology* **217**:3625-3639 https://doi.org/10.1083/jcb.201807019 | PubMed

Lang AE, Lozano AM (1998) Parkinson's Disease. *New England Journal of Medicine* **339**:1044-1053 https://doi.org/10.1056/NEJM199810083391506 | PubMed

Lappe-Siefke C, Goebbels S, Gravel M, Nicksch E, Lee J, Braun PE, Griffiths IR, Nave K.-A (2003) Disruption of Cnp1 uncouples oligodendroglial functions in axonal support and myelination. *Nature Genetics* **33**:366-374 https://doi.org/10.1038/ng1095 | PubMed

Lee T, Luo L (1999) Mosaic Analysis with a Repressible Neurotechnique Cell Marker for Studies of Gene Function in Neuronal Morphogenesis. *Neuron* **22**:451-461 https://doi.org/10.1016/s0896-6273(00)80701-1

Lesage S, Drouet V, Majounie E, Deramecourt V, Jacoupy M, Nicolas A, Cormier-Dequaire F, Hassoun SM, Pujol C, Ciura S, *et al.* (2016) Loss of VPS13C Function in Autosomal-Recessive Parkinsonism Causes Mitochondrial Dysfunction and Increases PINK1/Parkin-Dependent Mitophagy. *American Journal of Human Genetics* **98**:500-513 https://doi.org/10.1016/j.ajhg.2016.01.014 | PubMed

Love MI, Huber W, Anders S (2014) Moderated estimation of fold change and dispersion for RNA-seq data with DESeq2. *Genome Biology* **15**:1-21 https://doi.org/10.1186/s13059-014-0550-8 | PubMed

MacDonald JM, Beach MG, Porpiglia E, Sheehan AE, Watts RJ, Freeman MR (2006) The Drosophila Cell Corpse Engulfment Receptor Draper Mediates Glial Clearance of Severed Axons. *Neuron* **50**:869-881 https://doi.org/10.1016/j.neuron.2006.04.028 | PubMed

Morais VA, Haddad D, Craessaerts K, De Bock P.-J, Swerts J, Vilain S, Aerts L, Overbergh L, Grünewald A, Seibler P, *et al.* (2014) PINK1 Loss-of-Function Mutations Affect Mitochondrial Complex I Activity via NdufA10 Ubiquinone Uncoupling. *Science* **344**:203-207 https://doi.org/10.1126/science.1249161 | PubMed

Morais VA, Verstreken P, Roethig A, Smet J, Snellinx A, Vanbrabant M, Haddad D, Frezza C, Mandemakers W, Vogt-Weisenhorn D, *et al.* (2009) Parkinson's disease mutations in PINK1 result in decreased Complex I activity and deficient synaptic function. *EMBO Molecular Medicine* **1**:99-111 https://doi.org/10.1002/emmm.200900006 | PubMed

Munhoz RP, Moro A, Silveira-moriyama L, Teive HA (2015) Non-motor signs in Parkinson's diseasell: a review. *Arq. Neuropsiquiatr* **73**:454-462 https://doi.org/10.1590/0004-282X20150029 | PubMed

Muñoz-Braceras S, Tornero-Écija AR, Vincent O, Escalante R (2019) VPS13A, a closely associated mitochondrial protein, is required for efficient lysosomal degradation. *Disease Models & Mechanisms* **12** https://doi.org/10.1242/dmm.036681 | PubMed

Narendra DP, Jin SM, Tanaka A, Suen D.-F, Gautier CA, Shen J, Cookson MR, Youle RJ (2010) PINK1 Is Selectively Stabilized on Impaired Mitochondria to Activate Parkin. *PLoS Biology* **8**:e1000298 https://doi.org/10.1371/journal.pbio.1000298 | PubMed

Narendra DP, Youle RJ (2024) The role of PINK1–Parkin in mitochondrial quality control. *Nature Cell Biology* **26**:1639-1651 https://doi.org/10.1038/s41556-024-01513-9 | PubMed

Otto N, Marelja Z, Schoofs A, Kranenburg H, Bittern J, Yildirim K, Berh D, Bethke M, Thomas S, Rode S, *et al.* (2018) The sulfite oxidase Shopper controls neuronal activity by regulating glutamate homeostasis in Drosophila ensheathing glia. *Nature Communications* **9**:3514 https://doi.org/10.1038/s41467-018-05645-z | PubMed

Patel H, Ewels P, Manning J, Garcia MU, Peltzer A, Hammarén R, Botvinnik O, Talbot A, Sturm G, Bot N, *et al.* (2020) nf-core/rnaseq: nf-core/rnaseq. Zenodo. https://doi.org/10.5281/zenodo.1400710

Pech U, Janssens J, Schoovaerts N, Kuenen S, Aristoy CC, Gallego SF, Makhzami S, Hulselmans G, Poovathingal S, Davie K, *et al.* (2025) Synaptic deregulation of cholinergic projection neurons causes olfactory dysfunction across 5 fly Parkinsonism models. *eLife* **13**:RP98348 https://doi.org/10.7554/eLife.98348.3

Perkins LA, Holderbaum L, Tao R, Hu Y, Sopko R, McCall K, Yang-Zhou D, Flockhart I, Binari R, Shim HS, *et al.* (2015) The transgenic RNAi project at Harvard medical school: Resources and validation. *Genetics* **201**:843-852 https://doi.org/10.1534/genetics.115.180208 | PubMed

Picelli S, Björklund ÅK, Faridani OR, Sagasser S, Winberg G, Sandberg R (2013) Smart-seq2 for sensitive full-length transcriptome profiling in single cells. *Nature Methods* **10**:1096-1100 https://doi.org/10.1038/nmeth.2639 | PubMed

Pogodalla N, Kranenburg H, Rey S, Rodrigues S, Cardona A, Klämbt C (2021) Drosophila ßHeavy-Spectrin is required in polarized ensheathing glia that form a diffusion-barrier around the neuropil. *Nature Communications* **12**:6357 https://doi.org/10.1038/s41467-021-26462-x | PubMed

Pogson JH, Ivatt RM, Sanchez-Martinez A, Tufi R, Wilson E, Mortiboys H, Whitworth AJ (2014) The Complex I Subunit NDUFA10 Selectively Rescues Drosophila pink1 Mutants through a Mechanism Independent of Mitophagy. *PLoS Genetics* **10**:e1004815 https://doi.org/10.1371/journal.pgen.1004815 | PubMed

Poole AC, Thomas RE, Yu S, Vincow ES, Pallanck L (2010) The mitochondrial fusion-promoting factor mitofusin is a substrate of the PINK1/parkin pathway. *PLoS ONE* **5** https://doi.org/10.1371/journal.pone.0010054 | PubMed

Praschberger R, Kuenen S, Schoovaerts N, Kaempf N, Singh J, Janssens J, Swerts J, Nachman E, Calatayud C, Aerts S, *et al.* (2023) Neuronal identity defines α-synuclein and tau toxicity. *Neuron* **111**:1577-1590.e11. https://doi.org/10.1016/j.neuron.2023.02.033 | PubMed

Puri R, Cheng XT, Lin MY, Huang N, Sheng ZH (2019) Mul1 restrains Parkin-mediated mitophagy in mature neurons by maintaining ER-mitochondrial contacts. *Nature Communications* **10** https://doi.org/10.1038/s41467-019-11636-5 | PubMed

Purice M (2020) Olfactory receptor neuron (ORN) axotomy assay. *Bio-Protocol Preprint* bio-protocol.org/prep625

Purice MD, Ray A, Münzel EJ, Pope BJ, Park DJ, Speese SD, Logan MA (2017) A novel Drosophila injury model reveals severed axons are cleared through a draper/MMP-1 signaling cascade. *eLife* **6**:1-30 https://doi.org/10.7554/eLife.23611 | PubMed

Saab AS, Tzvetavona ID, Trevisiol A, Baltan S, Dibaj P, Kusch K, Möbius W, Goetze B, Jahn HM, Huang W, *et al.* (2016) Oligodendroglial NMDA Receptors Regulate Glucose Import and Axonal Energy Metabolism. *Neuron* **91**:119-132 https://doi.org/10.1016/j.neuron.2016.05.016 | PubMed

Schindelin J, Arganda-Carrera I, Frise E, Verena K, Mark L, Tobias P, Stephan P, Curtis R, Stephan S, Benjamin S, *et al.* (2009) Fiji - an Open platform for biological image analysis. *Nature Methods* **9** https://doi.org/10.1038/nmeth.2019

Slabbaert JR, Kuenen S, Swerts J, Maes I, Uytterhoeven V, Kasprowicz J, Fernandes AC, Blust R, Verstreken P (2016) Shawn, the Drosophila homolog of SLC25A39/40, is a mitochondrial carrier that promotes neuronal survival. *Journal of Neuroscience* **36**:1914-1929 https://doi.org/10.1523/JNEUROSCI.3432-15.2016 | PubMed

Smajic S, Prada-Medina CA, Landoulsi Z, Ghelfi J, Delcambre S, Dietrich C, Jarazo J, Henck J, Balachandran S, Pachchek S, *et al.* (2022) Single-cell sequencing of human midbrain reveals glial activation and a Parkinson-specific neuronal state. *Brain* **145**:964-978 https://doi.org/10.1093/brain/awab446 | PubMed

Soukup S, Kuenen S, Vanhauwaert R, Geens A, De B, Verstreken P (2016) A LRRK2-Dependent EndophilinA Phosphoswitch Is Critical for Macroautophagy at Presynaptic Article A LRRK2-Dependent EndophilinA Phosphoswitch Is Critical for Macroautophagy at Presynaptic Terminals. *Neuron* **92**:829-844 https://doi.org/10.1016/j.neuron.2016.09.037 | PubMed

Suárez-Pozos E, Thomason EJ, Fuss B (2020) Glutamate Transporters: Expression and Function in Oligodendrocytes. *Neurochemical Research* **45**:551-560 https://doi.org/10.1007/s11064-018-02708-x | PubMed

Tang FL, Liu W, Hu JX, Erion JR, Ye J, Mei L, Xiong WC (2015) VPS35 Deficiency or Mutation Causes Dopaminergic Neuronal Loss by Impairing Mitochondrial Fusion and Function. *Cell Reports* **12**:1631-1643 https://doi.org/10.1016/j.celrep.2015.08.001 | PubMed

Valadas JS, Esposito G, Vandekerkhove D, Miskiewicz K, Deaulmerie L, Raitano S, Seibler P, Klein C, Verstreken P (2018) ER Lipid Defects in Neuropeptidergic Neurons Impair Sleep Patterns in Parkinson's Disease. *Neuron* **98**:1155-1169.e6. https://doi.org/10.1016/j.neuron.2018.05.022 | PubMed

Velayos-Baeza A, Vettori A, Copley RR, Dobson-Stone C, Monaco AP (2004) Analysis of the human VPS13 gene family. *Genomics* **84**:536-549 https://doi.org/10.1016/j.ygeno.2004.04.012 | PubMed

Vilariño-Güell C, Wider C, Ross OA, Dachsel JC, Kachergus JM, Lincoln SJ, Soto-Ortolaza AI, Cobb SA, Wilhoite GJ, Bacon JA, *et al.* (2011) VPS35 mutations in parkinson disease. *American Journal of Human Genetics* **89**:162-167 https://doi.org/10.1016/j.ajhg.2011.06.001 | PubMed

Vilinsky I, Johnson KG (2012) Electroretinograms in Drosophila: A Robust and Genetically Accessible Electrophysiological System for the Undergraduate Laboratory. *The Journal of Undergraduate Neuroscience Education* **11**:149-157 http://fly.bio.indiana.edu/ | PubMed

Vonk JJ, Yeshaw WM, Pinto F, Faber AIE, Lahaye LL, Kanon B, van der Zwaag M, Velayos-Baeza A, Freire R, van IJzendoorn SC, *et al.* (2017) Drosophila Vps13 Is Required for Protein Homeostasis in the Brain. *PLOS One* **12**:e0170106 https://doi.org/10.1371/journal.pone.0170106 | PubMed

Vrijsen S, Vrancx C, Del Vecchio M, Swinnen JV, Agostinis P, Winderickx J, Vangheluwe P, Annaert W (2022) Inter-organellar Communication in Parkinson's and Alzheimer's Disease: Looking Beyond Endoplasmic Reticulum-Mitochondria Contact Sites. *Frontiers in Neuroscience* **16** https://doi.org/10.3389/fnins.2022.900338 | PubMed

Weigert M, Schmidt U, Haase R, Sugawara K, Myers G (2019) Star-convex Polyhedra for 3D Object Detection and Segmentation in Microscopy. http://arxiv.org/abs/1908.03636

Wolf FA, Angerer P, Theis FJ (2018) SCANPY: large-scale single-cell gene expression data analysis. *Genome Biology* **19**:15 https://doi.org/10.1186/s13059-017-1382-0 | PubMed

Wong YC, Peng W, Krainc D (2019) Lysosomal Regulation of Inter-mitochondrial Contact Fate and Motility in Charcot-Marie-Tooth Type 2. *Developmental Cell* **50**:339-354.e4. https://doi.org/10.1016/j.devcel.2019.05.033 | PubMed

Wong YC, Ysselstein D, Krainc D (2018) Mitochondria–lysosome contacts regulate mitochondrial fission via RAB7 GTP hydrolysis. *Nature* **554**:382-386 https://doi.org/10.1038/nature25486 | PubMed

Wu B, Li J, Chou Y.-H, Luginbuhl D, Luo L (2017) Fibroblast growth factor signaling instructs ensheathing glia wrapping of Drosophila olfactory glomeruli. *Proceedings of the National Academy of Sciences* **114**:7505-7512 https://doi.org/10.1073/PNAS.1706533114 | PubMed

Wu CF, Wong F (1977) Frequency characteristics in the visual system of Drosophila: Genetic dissection of electroretinogram components. *Journal of General Physiology* **69**:705-724 https://doi.org/10.1085/jgp.69.6.705 | PubMed

Wu YE, Pan L, Zuo Y, Li X, Hong W (2017) Detecting Activated Cell Populations Using Single-Cell RNA-Seq. *Neuron* **96**:313-329.e6. https://doi.org/10.1016/j.neuron.2017.09.026 | PubMed

Yamano K, Wang C, Sarraf SA, Münch C, Kikuchi R, Noda NN, Hizukuri Y, Kanemaki MT, Harper W, Tanaka K, *et al.* (2018) Endosomal Rab cycles regulate Parkin-mediated mitophagy. *eLife* **7**:1-32 https://doi.org/10.7554/eLife.31326 | PubMed

Yildirim K, Petri J, Kottmeier R, Klämbt C (2019) Drosophila glia: Few cell types and many conserved functions. *Glia* **67**:5-26 https://doi.org/10.1002/glia.23459 | PubMed

Yun J, Puri R, Yang H, Lizzio MA, Wu C, Sheng Z.-H, Guo M (2014) MUL1 acts in parallel to the PINK1/parkin pathway in regulating mitofusin and compensates for loss of PINK1/parkin. *eLife* **3** https://doi.org/10.7554/elife.01958 | PubMed

Zimprich A, Benet-Pagès A, Struhal W, Graf E, Eck SH, Offman MN, Haubenberger D, Spielberger S, Schulte EC, Lichtner P, *et al.* (2011) A mutation in VPS35, encoding a subunit of the retromer complex, causes late-onset parkinson disease. *American Journal of Human Genetics* **89**:168-175 https://doi.org/10.1016/j.ajhg.2011.06.008 | PubMed

Ghezzi L, Kuenen S, Pech U, Schoovaerts N, Kilic A, Poovathingal S, Davie K, Lamote J, Praschberger R, Verstreken P (2026) Parkinson's Disease-Associated Pink1 Loss Disrupts Ensheathing Glia And Causes Dopaminergic Neuron Synapse Loss. NCBI Gene Expression Omnibus. ID GSE322929 https://www.ncbi.nlm.nih.gov/geo/query/acc.cgi?acc=GSE322929

Janssens J, Pech U, Aerts S, Verstreken P (2025) Rescuing early Parkinson-induced hyposmia prevents dopaminergic system failure [fruit fly]. NCBI Gene Expression Omnibus. ID GSE228843 https://www.ncbi.nlm.nih.gov/geo/query/acc.cgi?acc=GSE228843

Peer reviews

Reviewer #1 (Public review):

Summary:

This study investigates the impact of Pink1 loss on glial function and neuronal health in a Drosophila model, highlighting the role of mitochondria-organelle contacts and key genes such as Ccz1, Vps13, Mon1, and Rab7. The work provides insights into cellular processes underlying neurodegenerative diseases, with a focus on glia-neuron interactions.

Comments on revised version:

I have reviewed the revised manuscript and the authors' responses to previous comments. The authors have addressed the key concerns raised by the reviewers, including validation of the Mz-GAL4 line and additional control experiments. The remaining issues caused by experimental constraints are understandable in this study.

However, several concerns remain. Notably, some key results were removed due to the use of inadequately characterized fly lines, and the lack of follow-up experiments to address these issues raises concerns regarding the validity and reliability of the findings. Furthermore, the absence of experiments examining Rab7-mediated membrane trafficking or the interactions between mitochondria and lysosomes in the Pink1 mutant presents a limitation. These missing elements reduce the clarity and interpretability of Figure 5 for readers.

On a positive note, the data showing that reducing Vps35/Vps13 enhances neuronal function and rescues Pink1 mutant phenotypes in ensheathing glia contributes meaningfully to the overall narrative.

Despite these limitations, this research addresses an important question in neuroscience using the Drosophila model. It provides a novel perspective on Parkinson's disease and neurodegeneration by exploring mechanisms underlying Pink1 loss and suggesting a role for mitochondria-organelle interactions in ensheathing glia, potentially regulated via Vps35/Vps13-mediated pathways.

Overall, the current version presents a clear and meaningful contribution to the field.

https://doi.org/10.7554/eLife.105386.2.sa2

Reviewer #2 (Public review):

Summary:

This study proposes a novel role for ensheathing glia (EG) in a Pink1-model of Parkinson's disease and shows that this cell population exhibits the highest number of DEG in a pre-symptomatic stage. In the olfactory system, there seems to be morphological changes in this cell-type that resembles an 'activated' state and the authors further show that the neuronal loss of Pink1 is responsible for this defect. The authors go on to show that manipulation of Pink1 in EG also leads to some defects in the visual system and in the dopaminergic neurons (DAN) that innervate the mushroom body (MB), and performed a screen based on the 'on-transient' defect of the ERG to identify potential genes that may modulate the function of EG in synaptic regulation. They focus on several genes related to vesicle trafficking including Vps13, and Vps35 and performed some additional experiments in the visual system and MB

to propose the role of vesicle/lipid trafficking in EG as an important factor for PD pathogenesis.

Strengths:

The study proposes functional and mechanistic connections between several genes that have been linked to PD (PINK1, VPS35 and VPS13A/C). I feel that the data presented in Figure 1-Figure 3C are performed with rigor and are convincing/novel. The selection of Drosophila to study the questions is also a strength and the lab has extensive experiences in this field and model organism.

Weaknesses:

In this revised manuscript, a number of concerns raised by this and the other reviewer was addressed. The authors now admitted that some of the genetic reagents used in their screen and follow up assays were inappropriately utilized, and changed the latter half of the paper (Fig 3D-F4) quite significantly (e.g. now only 1 gene is considered as a hit in Fig3D, analysis of several genes in Fig4 have been removed and replaced by some experiments performed on Vps35). The transition between Figure 3D and Figure 4 is quite abrupt, and they don't seem to follow up on the CG17660 (the single hit from their screen, which is not further validated so it is not clear whether this genetic reagent is clean or not) and the effect of Vps35 RNAi in synaptic phenotype. Therefore, there is still a weakness in Figure 3D-Figure 4, which weakens the paper, especially since the new model diagram the authors provided in Figure 5 is not really investigated at the molecular level.

https://doi.org/10.7554/eLife.105386.2.sa1

Author response:

The following is the authors' response to the original reviews.

> ***Public Reviews:***
>
> ***Reviewer #1 (Public review):***
>
> *Summary:*
>
> *This study investigates the impact of Pink1 loss on glial function and neuronal health in a Drosophila model, highlighting the role of mitochondria-organelle contacts and key genes such as Ccz1, Vps13, Mon1, and Rab7. The work provides insights into cellular processes underlying neurodegenerative diseases, with a focus on glia-neuron interactions. While the findings are promising, the study lacks critical controls, detailed mechanistic evidence, and explanatory figures to strengthen its claims.*
>
> *Strengths:*
>
> *(1) The study addresses an important topic in neuroscience, exploring the mechanisms of Pink1 loss, which has implications for Parkinson's disease and neurodegeneration.*
>
> *(2) The focus on mitochondria-organelle contacts and their regulation by Rab7-mediated pathways is novel and provides a potential mechanism for neuronal dysfunction.*
>
> *(3) The identification of key genes (Ccz1, Vps13, Mon1, Rab7) and their potential roles in Pink1-related pathways adds valuable knowledge to the field.*
>
> *(4) The manuscript uses a combination of genetic tools, Drosophila models, and functional assays to approach the problem from multiple angles.*

> *Weaknesses:*
>
> *(1) Specificity of Mz-Gal4: The study lacks validation of Mz-Gal4 specificity, as it may also drive expression in a few neurons or other types of glia. Additional control experiments using nls-GFP with Elav, Repo, or Draper antibody staining or alternative glial drivers would be helpful.*

We have addressed this issue of Gal4 driver specificity based on new experiments in the revised manuscript.

> *(2) DLG staining is central to the story but is not well-supported by high-resolution Z-stack imaging, which should be included in the supplementary figures.*

We have included these in the supplement.

> *(3) The manuscript does not confirm whether the candidate RNAi (Ccz1, Vps13, Mon1, Rab7) directly influence Rab7-mediated membrane trafficking or mitochondria-lysosome contacts in Pink1 mutants.*

This is indeed the case. These more mechanistic experiments were not yet performed.

> *(4) Using ERG as a readout for EG effects in the antenna is not a direct or appropriate assay. Alternative functional assays relevant to antenna glia should be considered.*

We made the assumption that ensheating glial function is conserved across brain regions and now make this explicit in the reworded manuscript.

> *(5) A graphical explanation of the interactions and functions of the candidate genes in Pink1 KO mutants is missing. This would greatly enhance the manuscript's clarity.*

We have included such a scheme in the new manuscript.

> *(6) The study lacks details on sample sizes, effect sizes, and reproducibility, which are necessary for robust conclusions.*

We have included these essential data in the reworked document.

> *(7) There are repeated words on page 3 ("olfactory Olfactory Receptor Neurons") and a lack of explanation in Figure 3C regarding the most up-regulated and down-regulated genes and the significance of large red dots.*

We have included the requested information.

> ***Reviewer #2 (Public review):***
>
> *Summary:*
>
> *This study proposes a novel role for ensheathing glia (EG) in a Pink1-model of Parkinson's disease and shows that this cell population exibits the highest number of DEG in a pre-symptomatic stage. In the olfactory system, there seems to be morphological changes in this cell-type that resembles an 'activated' state and the authors further show that the neuronal loss of Pink1 is responsible for this defect. The authors go on to show that manipulation of Pink1 in EG also leads to some defects in the visual system and in the dopaminergic neurons (DAN) that innervate the mushroom body (MB), and performed a screen based on the 'on-transient' defect of the ERG to identify potential genes that may modulate the function of EG in synaptic regulation. They focus on several genes related to Rab7/Vps13, and performed some additional experiments in*

the visual system and MB to propose the role of vesicle/lipid trafficking in EG as a important factor for PD pathogenesis.

Strengths:

The study proposes functional and mechanistic connections between several genes that have been linked to PD (PINK1, VPS13A/C). I feel that the data presented in Figure 1 and Fig3A-C are performed with rigor and are convincing/novel. The selection of Drosophila to study the questions is also a strength and the lab has extensive experiences in this field and model organism.

Weaknesses:

There is one fundamental concern I have with the genetic experiments performed in this paper (especially in Fig 3D and Fig4, see major issue #1), and I feel that there is a bit of a disconnect between the EG 'activation' phenotype the author show in the olfactory system and the other two neuronal systems (visual system, MB DAN) that the authors investigate see major issue #2). Also, there are quite a bit of information that is not provided in the manuscript (see major issues #3 and #4), which makes me difficult to judge the rigor and interpretation of several experiments.

Major Concern #1: A number of lines used in this study are referred to as "RNAi" lines but when I look at the actual genotypes of reagents listed in the table in the METHODS section, many are actually NOT RNAi lines. Quite a few lines, including lines that the authors use as RNAi against Ccz1, Rab7 and Mon1, are gRNA lines for the TKO (TRiP-CRISPR knockout) system. While these reagents can theoretically knock-out these genes in somatic cells if used in combination with UAS-Cas9, there is no mention that UAS-Cas9 was used in this work throughout the manuscript. Hence, when these lines are just crossed to GAL4 with or without the Pink1 mutant, they shouldn't be having any effects. Similarly, the strongest hit from their screen was a TOE (TRiP-CRISPR Over Expression) gRNA against PIG-A, which could allow overexpression of PIG-A if there is a UAS-dCas9::VP64. However, I also do not see any mention that such activator was introduced into the crossing scheme. Considering that 3 of the 4 'hits' from their screen are not RNAi lines, I am quite skeptical of the study. Similarly, except for Vps13, all reagents used in Fig4 are TKO gRNA lines. Therefore, if this experiment was conducted without an UAS-Cas9, most of the data shown here are problematic. Also, note that several of the 'RNAi' lines listed in the Table in the METHODS section are actually MiMIC alleles. While some MiMIC lines could function as strong LOF alleles (if they are inserted in the exon or in an intron of the gene in the same orientation as the gene), some of the lines are not expected to affect gene function (e.g. FASN2 and CG17712, MiMICs are in introns and face the opposite orientation). Hence, the rationale of including these reagents in the screen doesn't make much sense. The description of the modifier screen should be much more detailed in the RESULTS and METHODS section and if the UAS-Cas9/dCas9::VP64 transgenes were not introduced when the TKO/TOE reagents were utilized, what can be concluded?

In addition, for the 4 genes that the authors further study in Fig4, there are many other reagents that the authors can use, including mutant alleles, previously characterized RNAi lines (e.g. Vps13) and dominant negative/constitute active lines (e.g. especially for Rab7). The authors should validate their results with independent reagents to really convincingly show that the same conclusions can be drawn for the Vps13/Rab7 related genes since this is the key takeaway message of this paper.

Also, they do not show whether the manipulation of these genes in a wild-type background (they only show what happens in Pink1 mutants) affect ERG and MB DAN

> *synapse morphology. If these manipulations alone dramatically affect these phenotypes, it would be very difficult to interpret their data.*

We sincerely thank the reviewer for spotting this major oversight regarding the use of the TKO (TRiP-CRISPR knockout) and TOE (TRiP-CRISPR Over Expression) systems and the MiMIC alleles. As the reviewer pointed out, these lines were not used as intended, therefore our results and conclusions regarding the genetic interactions between Pink1 and several genes (PIG-A, Rab7, Ccz1, CG10646, Mon1, FASN2, CG17712), are incorrect and based on a technical mistake. These results were removed from the manuscript. While our mistake compromises the data regarding PIG-A, Rab7, Ccz1, CG10646, Mon1, FASN2, CG17712, it does not affect the results and conclusions for most of the genes of the screening and for Vps13 where we did use RNAi lines.

Also, in the reworked manuscript, we provide additional evidence that modulation of vesicle trafficking proteins involved in mitochondria–endoplasmic reticulum (ER) membrane interactions, such as Vps13 and Vps35, influences neuronal function and rescues *Pink1* mutant phenotypes when selectively downregulated in EG.

> *Major Concern #2: In Figure 1, the authors show some morphological evidence that EG are 'activated' in Pink1 mutants, but whether the same phenomenon occurs in the visual system and in the MB is not shown. Since all of the studies in Fig3D and Fig4 are done in the visual system and MB, it is not clear whether the visual system and MB phenotypes are related to 'activation' of EG.*
>
> *Also, in the RNA-seq data in Fig1A and Fig3C, is there any molecular evidence that EG are indeed 'activated'? The only evidence that the authors show to state that EG are 'activated' in young Pink1 null animals is based on increased CD8::GFP staining in the olfactory system.*
>
> *The authors cannot draw a strong conclusion that indeed EG are 'activated' based on these data (e.g. perhaps the expression level of CD8::GFP is just increased). Additional evidence that the EG are 'activated' could be provided by looking at the increase in Draper intensity (as reported by Doherty et al. and MacDonald et al. that the authors cite), not only in the olfactory system, but also in the visual system and in the MB. It would also be informative if the authors can look at morphology of the EG in the visual system and MB to convincingly that the data shown in Fig4 is relevant to EG 'activation'.*

In line with the identification of DEG across the ensheating glia cluster in our single cell sequencing (where we did not distinguish between EG of different brain regions) we made the assumption that EG-(dys) function is consistent in the *Pink1* mutant and conserved across brain regions. Nonetheless, to make clear that we did not consistently analyze EG morphology in the different brain regions that we probed in functional assays, we added a note in the manuscript. Furthermore, we also toned down our conclusion that the EG in *Pink1* mutants are in an activated state: we note the similarity in phenotype in *Pink1* mutants and situations of neuronal damage (where EG are activated) but added that the phenotype in *Pink1* mutants may also be the result of the mere upregulation of GFP expression/fluorescence.

> *Major Concern #3: In Fig3, there is no clear explanation why they focus on the ON transients and ignore the OFF transients, and also why the difference in the depolarization is not quantified in Fig4.*

We included this explanation in the reworked manuscript: In the *Drosophila* ERG, the sustained depolarization primarily reflects phototransduction in photoreceptors (and is defective when photoreceptors degenerate), whereas the ON and OFF transients arise from second-order lamina neurons and are widely used as readouts of signal transfer. We wanted to assess function and focused on the ON transient because in general it provides an onset-locked, more robust readout of function (Vilinsky & Johnson, 2012).

> *Major Concern #4: While the authors claim that mz709-GAL4 is a EG specific driver, do the authors know that this is indeed true in the tissues and stages that are studied here? The Ito et al,. paper that is cited in the METHOD section has only looked at the expression of this reporter in embryonic and larval stages. The authors need to that the authors should validate their findings with an additional EG specific driver and/or provide additional data that mz709-GAL4 is indeed specific to EG in the adult fly brain and eye. If mz709-GAL4 is expressed in other cell-types, the interpretation of many of the data in this paper becomes quite questionable. I believe the data in Fig3B is suggesting that mz709-GAL4 is indeed specific to glia cells and not expressed in neurons, but whether this driver is truly specific to EG (and not in other glial types), especially in the visual system (including the lamina as well as in the eye), is not obvious.*

We labelled animals that express *UAS-HisTag-eGFP* (used also in our paper) under control of *MZ709-Gal4* with anti-Elav (a neuronal marker) and find no significant overlap (see below "recommendation for authors"), consistent with *MZ709-Gal4* not driving expression in neurons. This is consistent with previous published work: Indeed, *MZ709-Gal4* has been amply used in adult flies and shown to be ensheating glia-specific (Doherty et al., 2009; Li et al., 2023; Sehgal et al.,2018). In the lamina neuropil of the *Drosophila* eye, MZ709-Gal4 is expressed in the marginal glia (Stenesen et al., 2019) which are neuropil-associated glia and are equivalent to generic ensheathing glia (Kremer et al., 2017). *MZ709-Gal4* is also expressed also in satellite glia (Stenesen et al., 2019), but these glia enwrap the cell bodies of the lamina neurons and not the neuropil where synapses reside.

> ***Recommendations for the authors:***
>
> ***Reviewing Editor Comments:***
>
> *We strongly encourage you to very carefully edit this manuscript. The reviewers made many probing comments that you should consider carefully.*
>
> ***Reviewer #1 (Recommendations for the authors):***
>
> *(1) Validate the specificity of Mz-Gal4 by performing experiments with nls-GFP and Elav antibody staining to ensure there is no neuronal overlap. Additionally, consider using alternative glial-specific drivers, such as Repo-Gal4 or WG-Gal4, to confirm the findings.*

We expressed *HisTag-eGFP* (used also in our paper) under control of *MZ709-Gal4* and labelled fly brains with anti-Elav (a neuronal marker). We do not observe significant overlap between the labels indicating *MZ709-Gal4* does not express Gal4 in neurons (Supplementary figure 1).

As indicated, these observations are consistent with previous published work. *MZ709-Gal4* has been amply used in adult flies and shown to be ensheating glia-specific (Doherty et al., 2009; Li et al., 2023; Sehgal et al., 2018; Stahl et al., 2018). In the lamina neuropil of the *Drosophila* eye, *MZ709-Gal4* is expressed in the marginal glia (Stenesen et al., 2019) which are neuropil-associated glia and are equivalent to generic ensheathing glia (Kremer et al., 2017). *MZ709-Gal4* is also expressed also in satellite glia (Stenesen et al., 2019), but these glia enwrap the cell bodies of the lamina neurons and not the neuropil where synapses reside.

> *(2) Include high-resolution Z-stack imaging of DLG staining to strengthen the assessment of synaptic integrity and ensure the robustness of the conclusions. These images should be added to either the main or supplementary figures.*

We included 2 supplementary figures (2 and 3) showing Z stacks that were used to delineate regions of interest at the MBs for the quantification of dopaminergic neuron afferents invasion. Our approach is identical to the one we used in Kaempf et al. 2026 (Kaempf et al., 2026).

> *(3) Demonstrate whether the candidate RNAi (Ccz1, Vps13, Mon1, Rab7) directly influence Rab7-mediated membrane trafficking or mitochondria-lysosome contacts in Pink1 mutants. Use an appropriate method to confirm changes in organelle contacts in response to the RNAi treatments.*

Ccz1, Mon1 and Rab 7 were removed due to the technical mistake we made. We did confirm and maintain that Vps35 and Vps13 downregulation in EG rescues neuronal defects in *Pink1* mutants. In the reworked manuscript we present a possible mechanism that involves the role of Vps35 and Vps13 in regulating ER-mitochondrial contacts, in line with our previous work (Valadas et al., 2018), while not ruling out possible other mechanisms.

> *(4) Provide an alternative functional assay or evidence to support the use of ERG as a readout for EG effects in the antenna. Consider using a more direct assay relevant to antenna glia function.*

We agree that a more direct functional assay of antennal glia would be a nice addition (e.g., single-sensillum recordings or glial/ORN Ca^{2+} imaging). However, implementing such assays would require new experimental pipelines and substantial additional data generation that is beyond our current ability and the scope of this revision.

> *(5) Add a graphical illustration explaining the proposed mechanism of how Ccz1, Vps13, Mon1, and Rab7 function in Pink1 KO mutants, highlighting their interactions and roles within specific cell types.*

We included a schematic of our working model in Figure 5.

> *(6) Clarify Figure 3C by explaining the most up-regulated and down-regulated genes and the significance of the large red dots. This will enhance the interpretability of the data.*

We expanded the legend to this figure: The large red dots represent the genes that rescue $Pink1^{KO\text{-}WS}$ phenotype when downregulated, the dark green dots are the 50 top most deregulated genes (magnitude of deregulation) in EG in $Pink1^{KO\text{-}WS}$ compared to controls, while the light green dots represent whole the genes detected in our cell-type specific transcriptomic experiment.

> *(7) Correct repeated words on page 3 ("olfactory Olfactory Receptor Neurons") for clarity and consistency.*

Of course, sorry for this.

> *(8) Ensure that sample sizes, effect sizes, and the number of replicates are explicitly stated for all experiments. This information is essential for evaluating the robustness and reproducibility of the findings.*

We made sure we consistently added all this information in the revised manuscript.

> *(9) Verify and ensure that all data, reagents, and code used in the study are accessible and appropriately documented, in adherence with eLife's publishing policies.*

We made sure all data, reagents and code are available and/or properly described.

> *By addressing these recommendations, the authors will significantly improve the clarity, rigor, and reproducibility of the manuscript.*
>
> ***Reviewer #2 (Recommendations for the authors):***
>
> *Minor Points.*
>
> *(1) All figures seem to lack titles.*

We fixed this error.

> *(2) In the abstract, the authors say that Rab7 and Vps13 are mutated in PD patients but I couldn't find the reference/information for Rab7 (the authors do refer to papers that linked VPS13A/C variants to PD but no mention about RAB7A/B being linked to PD). Please discuss this in the paper or modify the abstract accordingly.*

We removed this statement for rab7 from the paper.

> *(3) When referring to the human gene, Pink1 should be written as PINK1 according to the HGNC nomenclature rules.*

We made this change.

> *(4) The authors say Vps13 has two mammalian orthologs but actually it has four (VPS13A/B/C/D). I guess two of the four is linked to PD so the authors should modify there statement to reflect this.*

This is a misinterpretation of what we meant and we have clarified our intention: *Drosophila* possesses 3 paralogues of Vps13 - Vps13, Vps13B, and Vps13D - which we also detected in our screening (Neuman et al., 2025; Velayos-Baeza et al., 2004; Vonk et al., 2017). Among these Vps13 is most similar to human VPS13A and VPS13C (Hanna et al., 2023; McEwan & Ryan, 2022).

> *(5) The abbreviation 'CNS' is used in the first page of the intro but I don't see it being spelled out as "central nervous system".*

We have spelled out central nervous system in the first page of the introduction.

> *(6) On the top of page 5, the authors state that they confirmed that the 'synaptic area of DAN show a decrease in aged (25 days) animals' but data is not shown. If they want to make a statement like this, I believe such data should be included in supplemental data. Since the phenotype in the aged animal is not relevant to this study, one could remove this statement regarding the aged animals if they prefer not to show the data.*

The decreased synaptic area of DAN in 25-day old *Pink1* mutants is shown in figure 2C-D of the manuscript and is consistent with data shown in (Kaempf et al., 2026).

https://doi.org/10.7554/eLife.105386.2.sa0